

ADA 039600

AD

MECHANICAL PROPERTIES OF ENERGETIC MATERIALS

Final Technical Report

by

Professor D. Tabor, Dr J.E. Field, Dr M.M. Chaudhri,
H.M. Hauser & R.G. Patel

JANUARY 1977

EUROPEAN RESEARCH OFFICE
223 Old Marylebone Road,
LONDON NW1 5TH, England

Contract number DA-ERO-75-G-008 *need*

Physics and Chemistry of Solids,
Cavendish Laboratory, ✓
Cambridge,
England

DDC
APPROVED
MAY 18 1977
RESOLVED
B
Jr

Approved for public release; distribution unlimited

No.
FILE COPY

UNCLASSIFIED

SECURITY CLASSIFICATION OF THIS PAGE (When Data Entered)

REPORT DOCUMENTATION PAGE		READ INSTRUCTIONS BEFORE COMPLETING FORM
1. REPORT NUMBER	2. GOVT ACCESSION NO.	3. RECIPIENT'S CATALOG NUMBER
4. TITLE (and Subtitle) MECHANICAL PROPERTIES OF ENERGETIC MATERIALS.		5. TYPE OF REPORT & PERIOD COVERED FINAL TECHNICAL REPORT, JULY 76 - JANUARY 77.
6. AUTHOR(s) PROFESSOR D./TABOR, DR. J. E./FIELD, DR. M. M./CHAUDRI, H. M./HAUSER R.G./PATEL		7. CONTRACT OR GRANT NUMBER(s) DAERO-75-G-008
9. PERFORMING ORGANIZATION NAME AND ADDRESS PHYSICS & CHEMISTRY OF SOLIDS CAVENDISH LABORATORY CAMBRIDGE, U.K.		10. PROGRAM ELEMENT, PROJECT, TASK AREA & REPORT NUMBER 6.11.02A-1T161102B31B 00-486
11. CONTROLLING OFFICE NAME AND ADDRESS U.S. ARMY R&S GROUP (EUR) BOX 65 FPO NEW YORK 09510		12. REPORT DATE JANUARY 1977
14. MONITORING AGENCY NAME & ADDRESS (if different from Controlling Office) 55p.		13. NUMBER OF PAGES 52
		15. SECURITY CLASS. (of this report) UNCLASSIFIED
		15a. DECLASSIFICATION/DOWNGRADING SCHEDULE
16. DISTRIBUTION STATEMENT (of this Report) APPROVED FOR PUBLIC RELEASE DISTRIBUTION UNLIMITED		
17. DISTRIBUTION STATEMENT (of the abstract entered in Block 20, if different from Report)		
18. SUPPLEMENTARY NOTES		
19. KEY WORDS (Continue on reverse side if necessary and identify by block number) P.E.T.N: RDX: SECONDARY EXPLOSIVES: INDUCED DECOMPOSITION: HMX		
20. ABSTRACT (Continue on reverse side if necessary and identify by block number)		

016 550

15

UNCLASSIFIED

SECURITY CLASSIFICATION OF THIS PAGE(When Data Entered)

This report discusses observations we have made which emphasize the importance of the mechanical properties of explosive samples in various initiation situations, and describes work on the drop-weight impact test, micro-particle initiation of explosives and stab-initiation. One of the main features of the drop-weight experiments was the use of high-speed photography to follow the many processes which take place before initiation. It was found that the sample may undergo plastic flow in bulk, show evidence of partial melting, and even (with PETN) melt completely. Initiation, when it took place, always did so after the plastic failure of the sample. In the micro-particle impact experiments the possibility of localized plastic flow was assessed; flow concentration by adiabatic shear was shown to be important during particle-impact initiation of some explosives. Experiments in which a conical strike initiated samples of primary explosive showed that the initiation mechanism was frictional: a model is presented which allows the temperatures generated during impact to be estimated. Section 3, describes three approaches which were used to study the frictional properties of a range of explosives, including PETN, HMX, RDX, silver azide and lead azide. Data are also presented on the hardness and shear strengths of these explosives. The fracture and decomposition behaviour of PETN is discussed in section 4. Mass spectrometry work below the melting point showed that sublimation and decomposition occurred concurrently. Decomposition began at 75°C. The activation energy for slow thermal decomposition between 75 and 130° was 192±5 kJ/mol l. Fracture of reactive solids is shown to produce decomposition. Thermal, fracture-induced and laser-induced decomposition studies on P.E.T.N. are described; differences in kinetics of decomposition are commented on. Finally, section 5 describes a detailed study of the thermal decomposition of the sensitizing explosive tetracene.

Abstract

The introduction to this report discusses observations we have made which emphasize the importance of the mechanical properties of explosive samples in various initiation situations. Section 2 describes work on the drop-weight impact test, micro-particle initiation of explosives and stab-initiation. One of the main features of the drop-weight experiments was the use of high-speed photography to follow the many processes which take place before initiation. It was found that the sample may undergo plastic flow in bulk, show evidence of partial melting, and even (with PETN) melt completely. Initiation, when it took place, always did so after the plastic failure of the sample. In the micro-particle impact experiments the possibility of localized plastic flow was assessed; flow concentration by adiabatic shear was shown to be important during particle-impact initiation of some explosives. Experiments in which a conical strike initiated samples of primary explosive showed that the initiation mechanism was frictional: a model is presented which allows the temperatures generated during impact to be estimated. Section 3, describes three approaches which were used to study the frictional properties of a range of explosives, including PETN, HMX, RDX, silver azide and lead azide. Data are also presented on the hardness and shear strengths of these explosives. The fracture and decomposition behaviour of PETN is discussed in section 4. Mass spectrometry work below the melting point showed that sublimation and decomposition occurred concurrently. Decomposition began at 75°C. The activation energy for slow thermal decomposition between 75 and 130°C was $192 \pm 5 \text{ kJmol}^{-1}$. Fracture of reactive solids is shown to produce decomposition. Thermal, fracture-induced and laser-induced decomposition studies on P.E.T.N. are described; differences in kinetics of decomposition are commented on. Finally, section 5 describes a detailed study of the thermal decomposition of the sensitizing explosive tetracene.

Table of Contents

Page No.

1. INTRODUCTION	
2. IMPACT OF EXPLOSIVES	
(a) Drop-weight impact	
Discussion	
(b) Particle impact; the role of localized plastic flow	
Initiation results	
(i) Single crystals	
(ii) Compacted explosives	
Adiabatic shear bands	
Localization of flow in compacted explosives	
Conclusions	
(c) Stab initiation of explosives	

ACCESSION for	
DTIS	White Section <input checked="" type="checkbox"/>
DDC	Defi Section <input type="checkbox"/>
UNANNOUNCED	<input type="checkbox"/>
JUSTIFICATION.....	
BY.....	
DISTRIBUTION/AVAILABILITY CODES	
Dist.	ATAIL. INC/SP SPECIAL
A	

3. FRICTIONAL PROPERTIES OF EXPLOSIVES

Introduction

Factors affecting the friction between surfaces

Materials and sample preparation

Results and experimental procedure

Configuration (a)

Configuration (b)

Configuration (c)

Conclusion

4. FRACTURE AND DECOMPOSITION OF PETN

Thermal decomposition

Fracture-induced decomposition of reactive crystals

Fracture-induced decomposition of PETN

Laser-induced decomposition of PETN

5. THERMAL DECOMPOSITION OF TETRACENE

Introduction

Experimental

Specific heat measurements

Heat of reaction

The effect of rate of heating on peak temperature

Kinetic parameters

(a) Non-isothermal methods

(i) Kissinger method

(ii) Ozawa method

(b) Isothermal methods

(i) Slow thermal decomposition

(ii) Ignition time

Discussion

References

Figure captions

1. INTRODUCTION

It is well known that the mechanical properties of explosives and propellants can have important effects on their safe handling and performance, particularly after periods of storage. Over the last few years we have studied the initiation of explosives for a variety of experimental situations. In many cases it was found that the mechanical properties of the samples were of great relevance in explaining the explosive behaviour. Research on (i) drop-weight impact, (ii) microparticle impact and (iii) stab initiation (all discussed in section 2) in particular emphasized the need to measure quantities such as hardness, yield strength, tensile strength, fracture surface energy and coefficient of friction. Some of these properties are not easy to measure with reactive materials. Consequently a certain amount of experimental ingenuity had to be used to devise suitable methods of measurement. Section 3 describes three approaches which were used to study the frictional properties of explosives. The techniques involved sliding (i) single crystals on single crystals, (ii) single crystals on glass and (iii) glass surfaces over thin films of explosive deposited on glass substrates. Data are also given on hardness and shear strength.

Although mechanical properties can frequently determine how energy is localized and "hot-spots" formed in an explosive the subsequent behaviour then depends on the thermal properties of the surrounding medium (specific heat, conductivity) and its explosive properties (decomposition and fast reaction kinetics). Our research in this area has made use of such techniques as (i) mass spectrometry, (ii) differential scanning calorimetry (D.S.C.) and (iii) thermogravimetric analysis. Results on the secondary explosive P.E.T.N. (pentaerythritol tetranitrate) are given in section 4. This section includes work on (i) slow thermal, (ii) fracture and (iii) laser induced decomposition. The fact that the fracture of a thermally unstable solid can produce gaseous decomposition products and reactive fracture surfaces we feel is important to many explosive situations.

Finally, section 5 describes our work on the decomposition of tetracene. Activation energies, the specific heat and the heat of reaction were all obtained using D.S.C.

2. IMPACT OF EXPLOSIVES

(a) Drop-weight impact

This research was discussed in detail in the final report of an earlier contract (1) and in a paper by Heavens and Field (2). A brief description of the experimental approach and results are included here since the work highlighted the major importance of the mechanical properties of the sample in this impact situation, and the benefits of high-speed photography.

High-speed photographic observation of the behaviour of the layer of explosive material during impact was achieved with the aid of impacting surfaces of toughened glass, allowing the impact process to be viewed in transmitted light. The arrangement is represented schematically in figure 1. The upper glass block G was held in the recess of the weight W with plasticine. The hardness of the glass was between that of stainless steel and hard steel, and with a fairly high impact energy (5.5kg hammer, 1m drop-height) it was possible to ignite PETN (pentaerythritol tetranitrate), HMX (octogen, cyclo-tetramethylene tetranitramine), nitrocellulose, blasting gelatine and

ammonium perchlorate, but not RDX (cyclonite, cyclotrimethylene trinitramine), tetryl (trinitrophenylmethyl nitramine) or TNT (trinitrotoluene).

The event was photographed at 5 μ s per frame with an AWRE C4 rotating mirror framing camera, which being of the continuous access type did not require synchronization. The duration of the light flash was fixed at 500 μ s, less than the period of rotation of the mirror (700 μ s), so that double exposure on the camera film was avoided.

Only one high-speed sequence, figure 2, is included in this report (for others see references 1, 2). The sample is a thin layer of PETN of mass 14mg, and the sequence represents the final stages of compression of the layer, some 200 μ s after the initial instant of impact. At this point the layer, which has become compressed to a pellet of almost single crystal density, starts to undergo severe plastic deformation. In frames 2-6 high-speed (150m/s) jetting occurs and the layer becomes translucent. In frames 5 and 6 a wave-like structure can be seen developing within the layer. At frame 7 the layer suddenly becomes completely transparent and starts to flow very rapidly (300m/s), indicating that the layer has melted. Three ignition sites appear in frame 9, followed by growth reaction at 300-400m/s (the central spot D which persists in frames 7 to 9 is a defect in the glass; the ignition site I is to the left of this).

RDX showed similar behaviour to that of PETN, but did not reach the stage of melting completely and no ignition sites were observed. H.M.X. exhibited some plastic flow, but no melting, before ignition. Other explosives which flowed plastically before ignition included ammonium perchlorate, nitroglycerine, nitrocellulose, blasting gelatine and mining explosives. None of the aromatic secondary explosives tetryl, picric acid (trinitrophenol) or TNT could be ignited between glass anvils. These materials showed comparatively little tendency to flow. Of particular interest were results with silver azide and lead azide which also failed to initiate! They did not flow plastically and it is probable that their unexpected insensitiveness in this test, also noted by Russian workers (3), is peculiar to the perpendicular impact situation.

Pressure-time curves for the impact process were obtained with the aid of a Philips etched-foil resistance-wire strain gauge G (figure 3). The output from the gauge was connected to a Tektronix 551 double-beam oscilloscope, triggered independently by means of an electrical contact made by the falling steel weight W. In experiments with explosive samples the instant of ignition was registered on the second beam of the oscilloscope using either a transient light detector or a simple electrical circuit to detect the explosion.

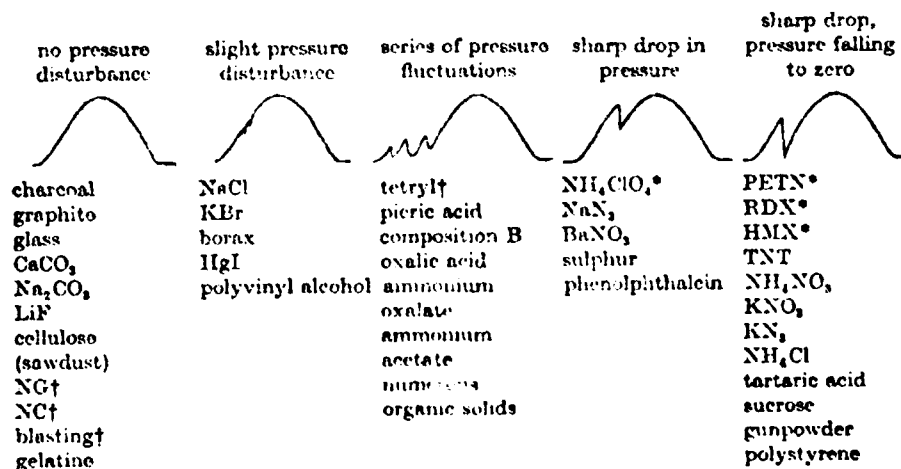
A few traces for explosive materials are given in figure 4. The solid secondary explosives all showed evidence of mechanical failure during impact. At low impact energies the samples did not ignite, but above a certain critical impact energy, dependent on the material, the sample ignited, and the lower traces of oscillograms for PETN, HMX, RDX and ammonium perchlorate showed that ignition occurred close to the instant of the sharp drop in pressure (figure 4a).

Sharp drops in pressure during the impact of PETN at the instant of ignition were first observed by Ljungberg in 1958 (4), who suggested (we think wrongly) that the drop in pressure was caused by the explosion, as a result of the rapid expansion of the reaction products or the removal of the

layer of material that had been sustaining the pressure. Most of the traces obtained by us indicated that the explosion occurs shortly after, or possibly during, the drop in pressure; consequently the pressure drop is due to mechanical failure of the sample, irrespective of whether or not ignition occurs. Figure 4b shows an example of a trace in which the instant of ignition occurs 30 μ s after the drop. Furthermore, if a relatively large sample was subjected to impact, the explosion destroyed the strain gauge and at the instant of explosion the trace left the scale as in figure 4d. It is clear from this trace that the pressure drop occurred well before the explosion, and that the effect of the explosion was to cause a sharp increase, not decrease, in pressure.

To avoid the possibility of a time lag between the instant of the explosion and the signal from the photocell, an electrical method was substituted, making use of the short-circuit between the steel rollers R2 and R3 resulting from the explosion. With this method a time lag of about 10 μ s was generally observed between the pressure drop and the explosion (figure 4d). Table 1 summarizes our results.

TABLE 1. THE TYPES OF PRESSURE-TIME CURVES SHOWN BY VARIOUS MATERIALS SUBJECTED TO IMPACT



* These materials ignited at the instant of the pressure drop.

† These materials ignited, but not at the instant of a pressure drop.

Discussion

Our photographic work revealed several phenomena including plastic flow, fusion (of PETN and RDX), jetting, wave formation, melting and ignition. The experiments, which included work on inert solids, showed that the sharp pressure drop was associated with plastic yielding of the layer. Figure 5 shows a radius-time plot for the impact of a layer of PETN; the first discontinuity AB is due to yielding of the layer, the second CD occurs upon melting. It is after the layer fails plastically that a permanent energy loss passes into the sample from the hammer. This energy heats the sample and is evidently sufficient to melt PETN. The factor of prime importance is the plastic failure of the sample which occurred in all cases where ignition was recorded.

It is clear that for plastic flow of the sample to occur, the impact pressure must attain the yield strength of the layer p_y , which is determined by the uniaxial field stress of the material σ_y and the thickness

h and diameter d of the layer. Application of the Mises yield criterion to a thin layer between two rigid cylindrical punches gives the following relation between these quantities (Schroeder & Webster 5):

$$P_y = \sigma_y \left(1 + \frac{d}{3\sqrt{3}h} \right) \quad (1)$$

This indicates that the thinner the layer, the higher the pressure necessary to make the material flow.

Equation 1 is useful in explaining size effects which occur with impacted explosive samples. For example the behaviour of PETN illustrated in fig. 2 occurred only with samples of mass 13mg or more. It was found that in the impact situation examined (5.5kg hammer from a height of 1m) samples of mass 10mg or less invariably failed to ignite. The same effect was observed with HMX, for which the 'critical mass' was about 18mg. Photographic sequences showed that the small samples showed very little tendency to flow. Chaudhri and Field (6) quote other evidence from Russian work (7, 8) in support of this idea for explaining size effects in their recent review chapter.

(b) Particle impact; the role of localized plastic flow

In these experiments impact was by small (up to $\sim 500\mu\text{m}$) high velocity particles. This impact situation has practical interest in the safe handling and use of explosives. Plant (9) has described how a high velocity fragment, either of inert or explosive material, from one exploding charge can initiate another. It is also known that when a crystal of lead azide explodes it produces numerous small fragments which move at high speed and can ignite other crystals placed some considerable distance away (10, 11). Another example is in an explosive "train" where one device triggers another by ejecting fragments at it. The present results give information on particle sizes and velocities which can cause initiation.

An additional advantage of using very small particles is that individual single crystals of explosive can be impacted. In fact a millimeter sized crystal appears "massive" to a micron-sized particle. Initiation was found to take place when critical conditions of particle size and velocity were exceeded. It was possible to examine the deformation produced when the impact conditions were just sub-critical and show that it was primarily plastic. Calculation showed that if the deformation energy were uniformly distributed around the indentation, only a small temperature rise would be produced. However, it is suggested that, because of thermal softening, the deformation is concentrated in narrow bands of material by adiabatic shear. The temperature rise in these regions can then be very high resulting in initiation.

This work is thought to be important because it again emphasizes the role of mechanical properties and the effect on initiation of the mode of plastic deformation. Details of this work were given in (1) and have been published by Winter and Field (12). The main features of the experimental approach and the results are outlined below.

Two sets of apparatus were constructed; one employed an electrostatic technique based on a design by Shelton, Hendricks, and Weurker (13) to

accelerate particles in the size range up to 50 μm . (See Winter 14). The velocities to which particles of various sizes accelerated are shown in figure 6; it can be seen that the smaller particles accelerate to higher velocities. Lead and silver azide crystals were glued to a rigid target rod and impacted by particles with sizes in the range from sub-micron up to 50 μm . Increased particle energies were obtained by an explosive driver technique, and the apparatus is shown schematically in figure 7. Particles of chosen size were placed on a 360 μm phosphor-bronze plate below which was a detonator. The sheet was of sufficient thickness not to perforate when the detonator was fired. The particle velocities were in the range 170 to 220 ms^{-1} and did not depend significantly on size and material. For a spall plate to target separation of 10mm, particles placed on the plate with a density of ~ 10 particles/ mm^2 resulted in ~ 4 impact sites/ mm^2 on the target.

Initially the explosive crystals were glued to the target rod. However, a possible objection to this was that gas bubbles could be trapped beneath a crystal and during impact these could compress adiabatically and lead to initiation. To prevent this possibility some of the silver azide crystals were mounted as shown in figure 8 with crystals embedded in an epoxy resin ('araldite') which had been degassed in vacuum. When the 'araldite' had hardened it was polished down to expose a flat face of the crystal. Optical microscopy was used to confirm that gas was not trapped beneath the crystals. All impacts were at normal incidence on regions of the crystal at least twice as thick as the impacting particle diameter. To prevent impacts on thin regions the edges of the crystal were covered with a silicone adhesive compound, which had the added advantage that it caught any particles which landed in it, thus avoiding glancing impacts by reflection of particles from the 'mask'.

Single crystals of silver azide and lead azide and four types of compacted explosive were studied. These were lead azide, silver azide, lead azotetrazol and a mixture consisting of 50% lead dinitroresorcinate, 5% tetracene and 45% barium nitrate (L-mixture). 20mg portions of these explosives were pressed into 3.1mm diameter aluminium cup under a pressure of 0.14GPa. These specimens were fixed to the target rod so that the exposed face of the powder was impacted.

Glass, aluminium and tungsten spheres were used as projectiles; they were graded into sized lots using sieves.

Initiation Results

(i) Single crystals

For the very small particles which were accelerated by the electrical method the velocities achieved depended on the particle size (see figure 6). None of these particles caused initiation. However, with the second method larger particles could be fired and it was found that above a critical size particles impacting at $\sim 200\text{ms}^{-1}$ caused initiation of silver azide single crystals. For aluminium and glass particles the critical size was $80 \pm 10\mu\text{m}$. The crystals were initiated by 40 μm tungsten particles, the smallest that could be separated using the available sieves, but not by 10 μm tungsten particles (this size range is commercially available). The method of mounting the crystals did not appear to affect their sensitivity to impact initiation. Crystals impacted by particles near the critical size for initiation but which did not initiate were observed by optical microscopy. (The crystal

surfaces deteriorated rapidly making more detailed examination difficult). The impact sites were smooth plastic indentations; only occasional fractures were noticed. The deepest indentation observed was 25 μ m, indicating that this is close to the critical depth for initiation (figure 9).

Four lead azide crystals were impacted by 115 μ m glass particles; two crystals exploded and two did not. The crystals were about 20 μ m thick and in the cases when initiation was not produced severe fragmentation of the crystals occurred.

(ii) Compacted explosives

Aluminium particles were used for these experiments. The critical particle sizes for initiation are shown in table 2. It can be seen that the order of sensitiveness is (i) silver azide and lead azotetrazol (similar) (ii) lead azide (iii) L-mixture.

TABLE 2

Initiation of explosive compacts by aluminium particles impacting at a velocity of $\sim 200\text{ms}^{-1}$.

<u>Explosive</u>	<u>Critical Particle Diameter</u> (μm)
Silver azide	80 \pm 10
Lead azotetrazol	80 \pm 10
Lead azide	200 \pm 30
L-mixture (Lead dinitrorescorcinat, Barium nitrate and Tetrazene in the pro- portions 50, 45, to 5%)	230 \pm 30

For all of these compacts the deformation produced by just sub-critical impacts consisted of a depression with a granular surface. Their appearance suggested that a volume of material, about equal to the volume of the impacting sphere, had been dislodged.

Adiabatic Shear Bands

A deforming material can develop adiabatic shear bands if two conditions are fulfilled. First, a temperature rise needs to be produced: this will occur if the rate at which heat is generated by plastic flow is greater than that lost by conduction. Secondly, the rate of thermal softening within the bands should be greater than the rate of work hardening. The first experimental study of this phenomenon was made by Zener and Holloman (15) who used a punch geometry to study the effect of strain rate on the plastic flow of steel. At punch velocities above 3ms^{-1} bands of shear were observed within which strains of up to 100 were measured. It was considered that temperatures in excess of 1300K were produced in the bands. Since this early study, adiabatic shear bands have been observed in many materials and for a wide range of deformation situations. For example, Recht (16) compared the deformation properties of several metals by machining them on a lathe and

found that above a critical velocity, adiabatic shear bands appeared in the chips machined from the workpiece. Stock and Thomson (17) observed shear bands in aluminium alloys which had been impacted with spherical particles and flat-ended cylinders. Microstructural evidence was obtained that melting had taken place in the bands. There is evidence that adiabatic shear can occur in non-metals, particularly if the stress conditions are such that fracture is suppressed by a superimposed hydrostatic pressure. For example, Afanas'ev et al (18) impacted compacted ferric citrate trihydrate crystal compacts between anvils and found that dark brown glassy bands appeared in the impacted material. They suggest that melting had taken place along these bands as a result of heat generated by localized flow. There is some evidence that a similar deformation mechanism occurs in rock-like materials during earthquakes (McKenzie and Brune (19)). Experiments by Andrianova et al (20) and Rose (21) have shown that adiabatic shear can take place in some ductile polymers; in this work large temperature rises in the bands were measured. In recent experiments we have shown (22) that when brittle polymers such as polymethylmethacrylate (PMMA) are impacted adiabatic shear bands can be formed having a very similar distribution to those produced in metals.

Because of the small size of the indentations produced by 80 μ m particles and the explosive nature of the crystal it was impossible to observe whether or not adiabatic shear bands had formed in the impacted silver azide crystals. However, experiments with 80 μ m particles on PMMA and titanium gave similar impact craters to that illustrated in figure 9. An example of the deformation in a titanium specimen caused by the impact of a 4mm diameter sphere is illustrated in figure 10. With this size impacting body it was possible to study cross-sections in detail. In figure 10(a) dark bands can be seen intersecting the crater surface obliquely. These are adiabatic shear bands; one of these is shown at higher magnification in figure 10(b). The positions of the shear bands found in titanium impacted with large spheres (\sim 4mm diameter) are illustrated schematically in figure 11. In this model, it is assumed that the bands form by a mechanism involving the successive punching of progressively larger diameter cylinders of target material. It is assumed that similar bands could be produced in silver azide when a truly plastic indentation is formed at an impact strain rate. It is therefore suggested that the mechanism responsible for the initiation of silver azide crystals impacted at 200ms⁻¹ by 80 μ m Aluminium spheres is the production of high local temperatures as a result of adiabatic shear.

A detailed discussion of the adiabatic shear mechanism is given in reference 12. The conclusion is that at high strain rates silver azide, and possibly other explosive materials find it energetically favourable to shear on thin planes in the material where temperature softening (and possibly melting) take place and that temperature rises produced in this way can lead to initiation. The tendency to localized shear is assisted if the product pck (p = density, c = specific heat, k = thermal conductivity) is small, yield strength σ_y is high and melting point is low. As a class of materials explosives appear likely to be susceptible to adiabatic shear failure.

Localization of flow in compacted explosives

The observation that plastic flow can produce initiation in the spherical particle impact situation suggests that this mechanism might also be responsible for the initiation of compacted explosives. These consist of many small crystals pressed together; sometimes sensitising grit particles

are included. During deformation a large range of stress situations are produced on a micro-scale and there are several deformation processes which could take place leading to localized flow and possibly initiation. Various situations which can be envisaged are depicted in figure 12 (a to m) and are briefly listed below.

(i) Flow of individual grains

Some grains of explosive will experience large compressive stresses causing plastic deformation. Further localization could take place within individual grains by adiabatic shear processes (figures 12(a) and (b).)

(ii) Point contact situations

Situations which could lead to intense local deformation are illustrated in figure 12(c) to (f). Figure 12(c) and (d) represent the case when a hard particle indents a softer one. This would arise when there is more than one type of explosive or when grit particles are present. The process is similar to microparticle impact, and again it is possible for conditions favourable for adiabatic shear failure to arise. If there is a shear force as well as a normal force a ploughing action could take place. Localization will also occur if the 'point' is soft: Yuill (23) has shown that a liquid explosive can be initiated when a sharp metal point is stabbed through it on to a rigid plate. The temperature rise of the needle resulting from its plastic flow was sufficient to initiate the explosive. A similar situation could occur on a microscopic scale inside an impacted explosive compact (figure 12(e) and (f)). Shearing movements would enhance this effect.

(iii) Flow around sharp points

When a hard angular particle is embedded in a 'sea' of softer material undergoing shear deformation, flow concentrations will occur where the soft explosive flows past sharp points on the grit. This situation is similar to that illustrated in figure 12(j).

(iv) Spalling

If a cavity exists in an explosive through which a shock wave is passing, spalling can occur. The process, which is illustrated in figure 12(k) to (m) involves the breaking off of a fragment of explosive from one side of the cavity and its impact on the opposite side. On impact the situation will be similar to that occurring in microparticle impact, also to that represented in figure 12(c). This mechanism is similar to that suggested by Blackburn and Seely (24) to explain the initiation of PETN by high strength shocks.

(v) Viscous effects

Some explosives melt before they explode and in these cases the final stages of heating could take place as a result of viscous flow in the liquid phase. Heavens and Field (2), see also section 2a, have recently obtained photographic evidence of melting occurring in secondary explosives during 'drop-weight' impact. Rideal and Robertson (25) have suggested that if melting takes place, then flow of the liquid between grains produces hot spots by viscous heating. This process is illustrated in figures 12(h) and (i) and could occur when grains are sheared against one another or impacted together normally.

(vi) Frictional heating

Much theoretical and experimental work has been done to show that high local temperatures can be produced by friction (see for example, Bowden and Tabor (26), and Highway and Taylor (27)). Also Bowden, Stone and Tudor (28) have shown that frictional heating can lead to the initiation of some explosives. Basically, frictional heating will involve a combination of the processes discussed above. The present work supports the view that flow processes are more important in frictional initiation than, for example, fracture processes which also take place when brittle materials slide in contact.

Conclusions

If 'hot spots' are to be produced in an impacted explosive mechanisms must exist for localized dissipation of the impact energy. From experiments on compacted explosives it is difficult to unambiguously confirm or reject any of several possible initiation mechanisms. In this report experiments have been described in which silver azide single crystals were impacted by spherical particles. The stress system produced here is such that no significant fracturing occurs. The fact that no discontinuities are produced in the deforming region restricts the possible basic mechanisms of localization of energy to one, namely plastic deformation. It is shown that at high strain rates silver azide would be expected to deform in localized bands because of temperature softening. Silver azide melts before it explodes and the final stages of the heating must take place while the material is in the liquid phase. It is argued that the bands of molten explosive must initially be very thin and therefore continue to absorb a significant amount of energy. Since the results of the single crystal impact experiments described here give clear evidence in support of this mechanism, it seems likely that the process is also possible with compacted explosives. The result that compacts and single crystals of silver azide have similar threshold conditions, suggests that similar factors control initiation in the two cases. It is clear that in compacted explosives there are many situations which could lead to localized plastic deformation during impact loading. As a method of assessing the impact sensitivity of explosives generally, the method has a number of advantages over previous methods. It gives a well defined and reproducible impact situation which enables 'post mortem' examination of the impacted region. When the explosive is effectively 'massive', the size and shape of the sample do not affect the impact conditions. The method also gives results on critical particle sizes and velocities required to cause initiation and this has relevance to various practical situations.

(c) Stab initiation of explosives

We are concerned here with the initiation mechanism in a column of a compacted solid primary explosive when stabbed with a hard small-angle metallic conical striker. A model is presented which, for the first time, gives a quantitative estimate of the maximum temperature rise generated during the impact. The initiation mechanism is shown to be frictional.

The model is based on experimental investigations of the deformation behaviour of compacts of various reactive materials (silver azide, lead azide, lead azotetrazole) when hit with steel conical indenters. These

indenters had semi-apex angle 15° , were polished to a surface roughness of $5\mu\text{m}$ and had a flat tip of diameter $15\mu\text{m}$. The compact of a selected material (particle size up to $25\mu\text{m}$) was made in an aluminium cylindrical container, 4.3mm in diameter, 4.8mm high and 0.25mm wall thickness, by placing a quantity of the material in the container and compressing with a tightly fitting cylindrical punch to a load of 215kg . Indentations were carried out using an Instron machine (crosshead speed 0.166mm s^{-1}) and it was found that the load, L , and indenter penetration, x , were connected by

$$L = k_1 x^2 \quad (2)$$

where k_1 is a constant. An important observation was that during the indentation surface particles of the compact became firmly attached to the indenter tip and formed a thin coating on it (see figure 13).

Other studies on the deformation of compressed powders of inert materials with steel wedges (semi-apex angle 15°) revealed that the particle flow trajectory met the wedge surface at $\pi/2$, and this, combined with the observations described above (equation 2), suggests that the deformation of the compact by small-angle indenters can be described by plasticity theory (29) with a high value of the coefficient of friction between the indenter and the compact. This means that during the whole penetration period, the particles firmly attached to the indenter surface will rub against bulk particles with a relative velocity of $v(1 - \sin^2 15^\circ)$, where v is the indenter velocity. On the other hand, relative movement between the particles in other regions (that is, away from the indenter surface) of the compact will not occur for the whole period of the indentation. Moreover, as the thermal conductivity of the particles is much smaller than that of the indenter, the temperature generated at the metal/particle interface will be much smaller than at the particle/particle interface. Therefore, during indentation the maximum temperature rise will occur at the surface of the particles attached to the indenter.

To calculate the magnitude of the maximum temperature rise it is assumed that the particles attached to the indenter tip rub against a 'continuous plane surface' provided by the particles in the bulk. Now consider the case of one of the particles attached to the indenter. The frictional heat produced per second per unit area is

$$\frac{\mu v (1 - \sin^2 15^\circ) \omega_p}{A} \quad (3)$$

where μ is the coefficient of friction. A the area of contact, and ω_p the normal force on the particle. For a compact, the normal force for a particle of a given size can be calculated by assuming that the normal force on the surface of the indentation is uniform. The temperature rise can then be calculated by using the method of Blok (30); temperature rise from chemical reactions is neglected. If the contact area is circular of radius R , and q_1 and q_2 are the fractions of heat going into the particle and the plane surface, respectively, (that is, $q_1 + q_2 = 1$), the temperature rise ΔT at the centre of the contact area after a time t is given by

$$\Delta T = \frac{4}{\pi^2 \rho c} \int_0^t \frac{q_1 \mu v (1 - \sin^2 15^\circ) \omega_p (1 - \exp(-R^2 \rho c / 4 \lambda t))}{2A(4 \lambda t / \rho c)^{3/2}} dt \quad (4)$$

where ρ is the density, λ the thermal conductivity, c the specific heat and

$$q = \left[1 + \sqrt{\frac{\pi}{2} \frac{v(1 - \sin^2 15^\circ) R \rho c}{4\lambda}} \right]^{-1}$$

Now we can calculate the maximum temperature rise when a conical striker (semi-apex angle 15°) of mass M is dropped on to a compact for which the value of the constant k_1 (equation 2) has already been determined by experiment. The motion of the indenter will be given by

$$M \frac{d^2x}{dt^2} = -k_1 x^2 \quad (5)$$

This can be integrated to give the indenter velocity as a function of time. Then, by using equation (4) we can calculate the temperature rise at any time (or penetration) during the impact.

As an example, the temperature rise is calculated when a conical striker, mass 0.145 kg, strikes a compact of lead azide (compaction pressure 14.8 kg mm^{-2}) with an initial velocity of 0.5 ms^{-1} . Lead azide has been chosen since all the parameters in equation (4) are known and are:

- $m = 2.27 \times 10^{-3} \text{ kg}$ (for a particle $25 \mu\text{m}$ across)
- $k_1 = 3.53 \text{ kg mm}^{-2}$
- $c = 4.85 \times 10^2 \text{ J kg}^{-1} \text{ K}^{-1}$
- $\lambda = 16 \times 10^{-2} \text{ J m}^{-1} \text{ s}^{-1} \text{ K}^{-1}$
- $\rho = 4.7 \times 10^3 \text{ kg m}^{-3}$
- $\mu = 0.28$ (for the case of plastically deformed contact, see reference 31 and the next section of this report)
- $R = 6.4 \mu\text{m}$ (the value of R was obtained separately by compressing a lead azide particle against a rigid surface by a load equal to the normal force on a particle of that size during the indentation of the compact).

The results of the calculations are shown in figure 14. Curve a is for a 0.145-kg indenter, whereas curve b is that for a 0.290-kg indenter, but with the same initial kinetic energy as before. It will be seen from figure 14 that the temperature rise first increases quite rapidly with penetration, but its increase then slows down, and reaches a 'steady-state' value well before the indenter comes to rest. Note that the value of the steady-state temperature rise for the 0.145-kg indenter is 118 K, whereas it is 93 K for the 0.290-kg indenter and also that, for a given penetration, the 0.145-kg indenter gives a higher temperature. This explains the observations from stab sensitivity tests of an explosive carried out with indenters of different masses that the efficiency of initiation of reaction is higher for the indenter of smaller mass.

The steady-state temperature for the 0.145-kg indenter is 118 K plus the initial temperature of lead azide (293 K), giving 411 K; the ignition temperature of lead azide is $\sim 620 \text{ K}$ and therefore initiation of reaction is not to be expected, as is found experimentally. The same impact conditions are, however, just sufficient to cause initiation of reaction in lead azotetrazole whose ignition temperature is 493 K. The coefficient of friction for lead azotetrazole is twice that for lead azide, but the other physical properties of the two materials are similar. The estimated steady-state temperature is

~530 K. Therefore we expect a higher ignition probability for lead azotetrazole than for lead azide.

Our model also predicts that reaction initiation should occur at the indenter tip after the indenter has penetrated a certain minimum distance (for a given initial velocity of the indenter). High speed photographic studies of initiation of reaction in compacts of lead azotetrazole support these predictions, and a detailed account will be published elsewhere. A paper on the above work has been published by Chaudhri (32).

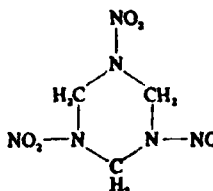
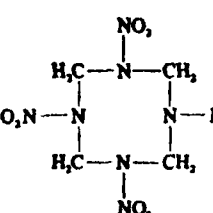
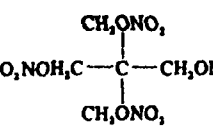
3. FRictionAL PROPERTIES OF EXPLOSIVES

Introduction

In some situations mechanical initiation of solid explosives has been considered to be due to friction (Bowden and Yoffe, 33). The quantitative assessment of models based on such a process requires a knowledge of the frictional force at the contact between the sliding solids. This section first outlines the factors which govern the frictional force between solids in the context of explosives and considers the effect of load, geometry, surface topography, material properties and temperature. It then describes how frictional properties can be obtained experimentally.

Friction measurements on explosive materials differ somewhat from measurements on other materials. In general, it is necessary to study very small amounts of material. This restriction is brought about by the fact that it is often not possible to grow large single crystals, and in addition safety considerations require that only small amounts of material are used. This constraint often necessitates the adoption of experimental procedures which measure the frictional force indirectly. Here we describe three types of experimental procedure: first the direct case where single crystals slide on single crystals (figure 15a); second where single crystals slide on smooth rigid substrates (figure 15b); and finally where a thin film of explosive material is sheared between smooth rigid substrates (figure 15c). These techniques and the calculation of the frictional force are described. Finally frictional and hardness data are presented for a series of explosive materials. The explosive substances studied are listed in table 3, together with a description of their physical form and their microhardness.

Table 3 : Explosive Materials

Explosive	Formula	Physical form at 20 °C	Vickers hardness of single crystals (kg mm ⁻²) at 20 °C	Melting point (°C)
Silver azide	AgN ₃	Crystals ~ 200 μm† in diameter	51.9 ± 2.6	251
α-lead azide	Pb(N ₃) ₂	Crystals ~ 200 μm† in diameter	119.7 ± 8.0	Explodes
Cyclotrimethylene trinitramine (RDX)		Crystals ~ 5 mm across	24.1 ± 0.8	202
Cyclotetramethylene tetranitramine (HMX)		Crystals ~ 5 mm across	41.3 ± 1	~279
Pentaerythritol tetranitrate (PETN)		Crystals ~ 5 mm across	17.9 ± 0.6	141

† Crystals of size 1 mm or greater are very difficult to grow.

Factors affecting the friction between surfaces

It is now generally accepted (26, 34) that when nominally clean bodies are slid over each other there are two major energy-dissipating processes; the adhesion component and the ploughing component. The two processes may be considered to act independently of each other. The adhesion mechanism suggests that when the surfaces are brought together the load is borne over a real area of contact A which is generally significantly less than the apparent area of contact, and that adhesive junctions are formed at these contacts. When the surfaces are moved over each other these junctions are repeatedly sheared and reformed. Thus energy is dissipated in a shear process within a narrow region close to the interface through a mechanism of plastic work or, in some cases involving brittle materials, by fracture work. If we assign to the junction a shear yield strength τ per unit area, then the frictional force F is simply

$$F = \tau A \quad (6)$$

if we assume that the real area of contact is not affected by the sliding process. This is generally not the case, and the area of real contact increases with the application of a sliding force (34). However, with our materials junction growth does not significantly affect the value of the coefficient of friction under most sliding conditions. This is due to the

fact that τ in equation (6) decreases with decreasing contact pressure (see below), and thus, at a constant load, while A increases, the contact pressure decreases and hence τA remains approximately constant.

The ploughing or grooving component of friction involves energy dissipation within a greater volume of material than is the case in the adhesion mechanism. The magnitude of this contribution depends to a limited extent on the mechanical properties of the material but is governed primarily by the geometry of the contact (33).

The ploughing component of friction becomes significant if a hard indenter or asperity ploughs its way through the surface of a softer solid. This would be the case when an indenter or rough surface which is appreciably harder than the explosive crystal moves over its surface. At very small loads where the contact deformation is wholly elastic the deformation contribution to the frictional force is approximately proportional to the product of some power of the elastic modulus and the fraction of energy lost through hysteresis during a deformation cycle (26). In general this contribution is always small compared with the adhesion component except for the case of lubricated sliding where the adhesional losses are small. At higher loads where extensive plastic deformation may occur the ploughing component may represent a significant contribution to work done during unlubricated sliding. Bowden and Tabor (35,36) have considered various cases of plastic ploughing assuming negligible interfacial adhesion and no 'pile up' of material ahead of the indenter. Their model for a simple case of a conical indenter of semi-apical angle θ yields a coefficient of friction, due to ploughing alone as $(2/\pi) \cot \theta$ and for $\theta=60^\circ$, $\mu_p \approx 0.32$ and $\theta=30^\circ$ (a rather sharp needle) $\mu_p \approx 1.1$. In this model no realistic estimate of the adhesional component of friction is possible but certainly the proportional contribution of ploughing to the sliding friction may be large. Currently there appears to be no simple way of assessing in detail the relative roles of the two components and their mutual interaction in lubricated friction where appreciable plastic grooving of one surface occurs and thus calculations of the magnitude of friction from first principles in these cases are imprecise.

In our experiments the ploughing component may be neglected so that the present paper deals only with the adhesion component of friction. This process is described by equation (6) and the rate of energy dissipation is related directly to the magnitude of τ . τ may be regarded as a part of the work done per unit sliding distance. For a given material τ is generally a function of temperature T , contact pressure P , and sliding velocity V . The area of contact A cannot, in general, be measured directly. It must be estimated using a model for the contact which takes into account the contact geometry, the surface topography, the load, the mechanical properties of the contacting solids, and the interaction of the load and the frictional force. Such models only provide an estimate of the contact area. However, where the contacting surfaces are smooth, the description of the contact is comparatively straightforward. If the contacting surfaces are loaded so that appreciable plastic deformation of one of both the substrates occurs then

$$A = W/p_0 \quad (7)$$

where W is the normal load and p_0 the flow or plastic yield stress of the softer material. The same relationship also holds for rough surfaces where

the individual asperities deform wholly in a plastic manner. The case of two elastically deforming substrates is more complex. With smooth surfaces, for example, a spherical surface on a flat surface or the equivalent case of two orthogonal cross cylinders of radii R_1 and R_2 , A is given by

$$A = \pi(MWR)^{2/3}$$

where

$$M = \frac{3}{4} \left[\frac{1 - \nu_1^2}{E_1} + \frac{1 - \nu_2^2}{E_2} \right] \quad (8)$$

ν and E are the Poisson's ratios and the Young's moduli respectively (37). The subscripts refer to two substrates. R is the mutual radius of curvature, $R_1R_2/(R_1 + R_2)$. For rough surfaces undergoing elastic deformation A is generally proportional to W such that

$$A \propto W^m \quad (9)$$

where m is an index between $\frac{2}{3}$ and 1 (38-40). The transition from elastic to plastic deformation in a multiple asperity contact has been considered by many authors (38,39) who have included both the mechanical and topographical properties of the solids.

The coefficient of friction μ may be calculated from equations (6), (7) and (8).

For elastic deformation on smooth surfaces

$$\mu = F/W = \tau(P,T,V)\pi(MR)^{2/3}W^{-1/3} \quad (10)$$

or generally $W^{(1-m)}$ where $(1-m)$ has values between $-\frac{1}{3}$ (for smooth surfaces) and zero (for certain types of rough surface).

For plastic deformation on both smooth and rough surfaces

$$\mu = \frac{\tau(P,T,V)}{P_0} = \frac{3\tau(P_0,T,V)}{H_V} \quad (11)$$

assuming that the local contact pressure is P_0 and that p_0 is given by $H_V/3$ (41) where H_V is the Vickers pyramid hardness (table 3). Both these assumptions are open to question: the local contact pressure for a multiple asperity contact may be somewhat less than p_0 (38), and for single crystals p_0 may be significantly less than $H_V/3$ (42).

We now consider how the contact conditions affect the magnitude of τ . Figure 15 shows three contact situations where ploughing is negligible. Our recent experiments (43) using configurations (b) and (c) (figure 15) have shown that with similar materials shear takes place within a narrow zone in the material. Results from PETN quoted later suggest that this is also the case for configuration (a). The energy dissipation process, and hence the magnitude of τ , will be similar in the three cases provided the contact conditions are the same. That is, they correspond to the same temperature T , sliding speed V , and contact pressure P . Other experiments on organic materials in similar configurations indicate that this is so and that the following empirical relationships apply (43-45).

$$\tau = \tau_0 + \alpha P \quad \text{at constant } T, V \quad (12)$$

$$\tau = \tau_0' \exp(Q/RT) \quad \text{at constant } P, V \quad (13)$$

$$V = \phi \tau^n \quad \text{at constant } T, P \quad (14)$$

where τ_0 , τ_0' , α , Q , ϕ and n are constants. Thus for a given substance, if the constants in equations (12), (13) and (14) are known as well as their variation with temperature, pressure and sliding velocity τ can be predicted for any sliding conditions. The real area of contact must then be estimated from a suitable contact model (in the case of smooth surfaces via equations (7) and (8) and the coefficient of friction estimated (equations 10 and 11)).

In spite of the assumption embodied in this approach, we shall see later that the estimated coefficient of friction is generally in agreement with the values obtained directly when single crystals slide on single crystals. The present account reports data for certain of the constants in equations (12), (13) and (14) for those explosive materials given in table 3. Where large crystals of the explosive material were available (PETN) all three sliding configurations shown in figure 15 were studied. In the case of the other explosives where the samples were much smaller, the configurations (b) and (c) of figure 15 were used. The data for PETN shown that the friction experiments described in figure 15 lead to similar coefficients of friction, and this supports earlier assumptions about the physical similarity of the three configurations.

Materials and sample preparation

Single crystals of HMX and RDX were kindly supplied by ERDE, Waltham Abbey, Essex. The single crystals of PETN and AgN_3 were grown by slow crystallization from acetone and aqueous ammonia solutions respectively. A diffusion technique was used to grow single crystals of $\alpha\text{-PbN}_6$. All the crystals were dried over silica gel prior to use.

The thin films were prepared on fired glass plates using a modification of the drop spreading technique proposed by Baier and Zisman (46). A small crystal ($\sim 10\text{-}100\mu\text{g}$ in weight) was placed on the glass surface, and a drop of solvent added. As the solvent spread over the glass it evaporated and deposited a thin layer of explosive material. The procedure was repeated until an area of suitable thickness was produced. The film thickness was estimated using multiple-beam interferometry: resolution was improved by coating the explosive film with a thin layer of silver. No marked variation in shear strength data was observed for films with thicknesses less than 300nm. The mean film thickness used was 200nm. The spreading solvents were: acetone for PETN; aqueous ammonia for AgN_3 ; and water for PbN_6 . All the films were dried over phosphorus pentoxide before use.

Results and experimental procedure

The three sliding configurations and a schematic diagram of the apparatus are shown in figure 15. The equipment used to measure the friction of the explosive materials has been described in detail elsewhere (43). The upper sliding member was supported in a load-cell at one end of a sensitive beam balance and loaded against the lower surface with a dead load W between 20mg and 20g. The lower surface was clamped on a

heating stage which was moved at a constant velocity by a hydraulic drive. Repeated traversals of the upper slider, of distance about 10mm, were made over the lower surface. Four sliding speeds were used: 0.04, 0.1, 0.2 and 0.4mm s⁻¹, the majority of the measurements were, however, conducted at 0.2mm s⁻¹. The load-cell provided a continuous measure of the frictional force which was generally reproducible to within $\pm 10\%$. In configuration (a) (figure 15) both surfaces were the explosive material PETN. The other configurations made use of flamed glass surfaces; in (b) an explosive crystal was slid over a glass flat; in (c) a thin film of the explosive ($\sim 200\text{nm}$) was deposited on the glass flat and a glass slider was slid over the film. Each configuration is now considered in detail.

Configuration (a)

Figure 16 shows the variation of μ with W for a single crystal of PETN sliding on another PETN crystal (figure 15(a)). The radius of curvature of the upper surface was estimated to be about 0.25mm before sliding. μ is independent of the load. We estimate, assuming a Hertzian contact of this radius for smooth surfaces, that gross plastic yielding of the contact will occur at approximately 1 g load. The fact that μ is independent of load suggests that the contacting surfaces are not smooth and that multiple contacts occur within the area of apparent contact; that is, m is close to unity in equation (9) and the contacts deform elastically for load less than about 1 g. Plastic deformation occurs at the contacts at higher loads and μ is given by equation (11). Again μ is independent of load.

In the plastic regime $\tau(P,T,V)$ may be estimated via equation (11) as $2.25 \times 10^7 \text{Nm}^{-2}$ (taking $p = p_0 = H_v/3 = 6 \times 10^7 \text{Pa}$).

Configuration (b)

Figure 16 shows data for single crystals of PETN, HMX, RDX, $\text{Pb}(\text{N}_3)_2$ and AgN_3 sliding against smooth fired glass substrates. At high loads μ tends to an asymptotic value for each crystal, while at light loads increases rapidly. At low loads the contacts are elastic, μ is therefore given by equation (10) (assuming a single asperity contact) until the contact pressure exceeds the yield pressure of the explosive crystal. Above the yield pressure p , μ is given by equation (11). Table 4 lists the values of $(1 - m)$ (equation (10)) derived from the data in figure 16 ($1 - m$) is obtained from a plot of $\log \mu$ against $\log W$ and is close to $-\frac{1}{3}$, indicating that the contact is singular and primarily elastic.

Table 4. Frictional properties at 20°C with sliding velocity of 0.20mms^{-1}

Column 1	2	3	4	5	6
Crystal μ	τ_0	α	$\mu_{\text{cal.}}$	μ	$-(1-m)$
PETN	0.40	$5.0 \times 10^6 \text{ Pa}$	0.45 ± 0.05	0.38 ± 0.02	0.40
HMX	0.55	—	—	—	0.29
RDX	0.35	—	—	—	0.26
AgN_3	0.40	$1.01 \times 10^7 \text{ Pa}$	0.42 ± 0.01	0.44 ± 0.02	0.37
$\text{Pb}(\text{N}_3)_2$	0.28	$2.9 \times 10^6 \text{ Pa}$	0.26 ± 0.04	0.26 ± 0.04	0.28

- Column 1. μ , coefficient of friction in configuration (b) at high loads taken from figure 16; marked plastic deformation of the contact occurs.
- Column 2. τ_0 , constant in equation (12) at 20°C; configuration (c).
- Column 3. α , constant in equation (12) at 20°C; data in figure 17; $\alpha \mu$ at high loads; configuration (c)
- Column 4. $\mu_{\text{cal.}}$, calculated coefficient of friction at high loads from equation (11) and figure 17.
- Column 5. μ , coefficient of friction for single crystal on single crystal.
- Column 6. m , index in equation (9); for smooth elastic contacts $(1 - m) = -0.33$.

Configuration (c)

In these experiments a flamed glass sphere of radius R is loaded against a thin film of the explosive material deposited on a flamed glass flat. We assume that the sheared area of film A is given by equation (8), where ν_1 , ν_2 , E_1 , E_2 are the elastic constants of the glass substrates. Further, we assume that no direct glass-glass contact occurs; this is confirmed by careful examination of the glass surface after sliding has occurred. The shear strength τ is then F/A , and the mean contact pressure P is W/A . The mean contact pressures covered in these experiments ranged from $4 \times 10^7 \text{ Pa}$ to $4 \times 10^8 \text{ Pa}$ by using loads between 20mg and 20g and radii between 2.5mm and 0.4mm.

Figure 17 shows τ against P for PETN, AgN_3 and $\text{Pb}(\text{N}_3)_2$ films. τ is a linear function of P ; the values of α and τ_0 (equation (12)) are listed in table 4. These data, α and τ_0 , may then be used to calculate the coefficient of friction at high loads (where plastic deformation of the contact occurs) in configuration 15(a) and (b) using equation (11) substituting the value of τ at p_0 ($Hv/3$). Table 4, (column 4) shows these calculated coefficients of friction (μ_{cal}). There is good agreement between the calculated values and those observed in configuration (b): see table 4 (column 1). Further, the values of μ for PETN in configurations (a), (b) and (c) are 0.4, 0.4 and 0.38 respectively, which confirms the similarity of the three sliding processes. Also, the value of τ at P_0 ($6 \times 10^7 \text{ Pa}$) in configuration (a) is $2.25 \times 10^7 \text{ Pa}$, which is close to the value of τ of $2 \times 10^7 \text{ Pa}$ obtained in configuration (c) at a mean contact pressure of $6 \times 10^7 \text{ Pa}$ (figure 18), which again emphasizes the similarity of the shear processes in the three sliding configurations.

The coefficient of friction at high loads may also be estimated directly from figure 17 and equations (11) and (12). Combining these equations

$$\mu = (\tau_0 + \alpha P_0)/P_0 = \tau_0/P_0 + \alpha$$

Comparing the values of α , τ_0 and P_0 (tables 3 and 4) we see that $P_0 > \tau_0$, and to a fair approximation the coefficient of friction μ is equal to α . The values of α and μ (at high loads) are compared in table 4 (columns 1, 3 and 4) and the agreement is seen to be quite good. This approach for estimating μ is very useful if P_0 is not known for the explosive material.

We now describe the effect of temperature on the shear strength τ . Figure 18 shows $\log \tau$ against $1/T$ for (equation 13) PETN and AgN_3 ; the values of Q are 6.0 ± 1 and $2.5 \pm 0.5 \text{ kJ mol}^{-1}$ respectively at a mean contact pressure of $6.7 \times 10^7 \text{ Pa}$. Other work on organic materials has shown that Q is not a strong function of pressure. Thus μ may be calculated for equations (10) and (11) provided that the temperature dependence of H_v (or P_0), E and v are known. Also shown in figure 18 is the temperature dependence of the Vickers pyramidal hardness of PETN (plotted as $\log H_v$ against the reciprocal of the absolute temperature). The apparent activation energy is $7.2 \pm 1 \text{ kJ mol}^{-1}$, close to the value of Q obtained for the temperature dependence of τ (equation 13) at constant contact pressure. The similarity between the values is not surprising, as both experiments monitor a yield process. The two experiments do however correspond to different strains and strains rates.

Finally, preliminary measurements of the velocity dependence of τ indicate that equation (14) holds reasonably well. With AgN_3 , $n = 6.3$ at 20°C and the contact pressure is $6.7 \times 10^7 \text{ Pa}$. Increasing the sliding velocity from 0.04 mm s^{-1} to 0.4 mm s^{-1} increases the estimated value of τ from $3.67 \times 10^7 \text{ Pa}$ to $5.40 \times 10^7 \text{ Pa}$, an increase of approximately 50%. Measurements were made on the effect of temperature on the indentation hardness for PETN.

Conclusions

Three approaches have been used to measure the coefficient of friction when single crystals of explosive are slid over each other. As well as the direct method of sliding single crystal on single crystal, a study was also made where single crystals were slid on smooth glass surfaces. The third method involved depositing the crystals as thin films on glass surfaces and then sliding the surfaces over one another. After certain assumptions had been made about the nature of the contact in the three cases and the mode of energy dissipation, it was possible to show that the thin-film technique was capable of predicting accurately the coefficients of friction obtained by the other techniques. This is consistent with the adhesion model of friction, which supposes that the energy of sliding is dissipated in a narrow zone close to the interface. The limiting factor in the use of the adhesion model is that it requires a knowledge of the actual area of contact. This quantity can only be estimated from models which include the topography and mechanical properties of the interface. In the current study single-crystal/single-crystal contacts were best modelled as multiple-asperity contacts in both the elastic and plastic deformation regimes. Single-crystal/smooth-glass contacts behaved as smooth contacts in the elastic regime and the coefficient of friction showed a marked load dependence.

Other measurements were made using thin-film techniques to study both the velocity and temperature dependence of the coefficient of friction. The shear strength decreases with temperature at approximately the same rate as the hardness for PETN. Thus one anticipates that the coefficient of friction will be independent of temperature over a wide range for single-crystal contacts. An increase in the interfacial shear strength with sliding velocity was observed for silver azide, but we have no data on the time-dependent hardness of this material. Thus a substantial part of the frictional work when bulk crystals are slid on themselves or on glass substrates can be interpreted using the adhesion model of friction. In general, those factors which increase the interfacial shear strength tend to increase the hardness of the material and hence reduce the area of contact. Hence the coefficient of friction is a constant at a given load. At high load the coefficient of friction becomes independent of load. The value of the coefficient varies somewhat between the explosive materials studied. No study was made of frictional anisotropy in these materials, but the film experiments suggest that marked anisotropy does not exist.

This study has completely neglected the ploughing component of friction. Thus the values of the coefficient of friction given in the paper must be considered as lower limits. In many cases ploughing may be negligible, but in certain cases the ploughing component may exceed the adhesion component. This would be the special case where a needle-shaped indenter slides over a bulk crystal at high loads. In this case it is not possible to compute simply the exact value of the ploughing component and the relative contributions of the ploughing and adhesional components of friction.

In a recent paper Winter and Field (12, see also section 2b above) considered the role of localized plastic flow in the impact initiation of explosives. They argue strongly for a mechanism of adiabatic heating in the shear plane and propose that the impact energy may be dissipated in various crystal configurations including those illustrated in figure 15. Further they note that energy dissipation involving plastic deformation of the bulk crystals may occur. While the present experiments do not attempt to deal with the mechanisms of initiation, the film data do however provide information on the rate of energy dissipation in localized zones, both at interfaces and within the bulk at elevated pressures, high strain rates and strains and moderate temperatures. The maximum sliding velocities in the film experiments (0.4 mm s^{-1}) was rather less than that suggested by Winter and Field for the onset of appreciable adiabatic heating. Most experiments were conducted at sliding speeds where such frictional heating was thought to be negligible.

Finally we note that the film technique is particularly suitable for studying the frictional properties and shear of explosives where large specimens of material are often not readily available and safety requirements necessitate working with small quantities of material.

4. FRACTURE AND DECOMPOSITION OF PETN

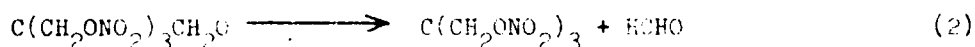
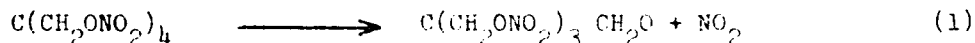
This is a widely used and important secondary explosive. We have made detailed studies of its mechanical, decomposition and explosive properties.

Thermal decomposition

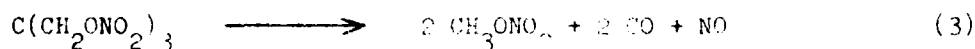
A study was made of the thermal decomposition of PETN below its melting point of 141°C using the Bendix RGA-1A time-of-flight mass spectrometer (for details see 1 or 47). Both sublimation and decomposition were found to occur concurrently. Decomposition begins at 75°C . An activation energy of 192 kJ mol^{-1} was obtained between 75°C and 130°C .

Mass spectra were taken at three temperatures (94° , 126° and 156°C). The mass spectrum of the decomposition products has major peaks in the low mass region below m/e 50. Prominent peaks are 18, 28, 29, 30, 44 and 46. The distribution was influenced by the temperature of decomposition. Below the melting point of PETN (141°C) a large amount of m/e 30 was found whereas at higher temperature m/e 18 and 28 dominated. These peaks correspond to the decomposition products: H_2O , N_2 , CO , HCHO , NO , CO_2 , N_2O and NO_2 . Because the crystal is recrystallized from acetone some of the trapped solvent also showed up in some of the spectra. The base peak occurs at m/e 43 due to the fragment ion CH_3CO^+ , but the amount is not significant in comparison with the decomposition products. Over the high mass region (i.e. $m/e > 50$) prominent peaks occurred at 55, 56, 76 and 85.

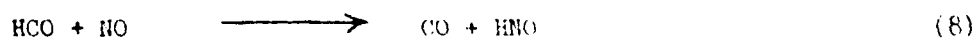
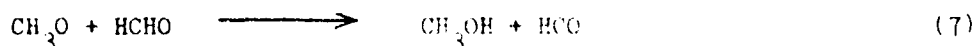
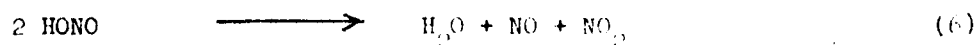
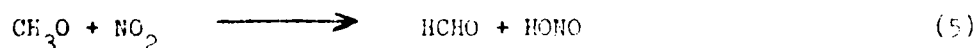
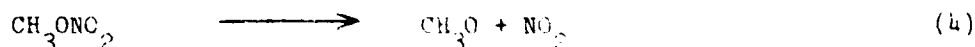
For mononitrate and nitrite esters, the primary process involves the rupture of the RO-NO_2 bond producing NO_2 or NO . The bond dissociation energy was estimated by Levy (48) to be ca. 173 kJ mol^{-1} . Our calculated activation energy of 192 kJ mol^{-1} for PETN is close to this and so from the energetic point of view, the primary process in the decomposition of PETN appears to be the rupture of one RO-NO_2 bond followed by the elimination of a neutral formaldehyde molecule (reactions (1) and (2)).



The relatively large amount of $\text{CH}_2\text{ONO}_2^+$ (m/e 76) present in the mass spectrum then suggests the ultimate break down of $\text{C}(\text{CH}_2\text{ONO}_2)_3$ as in reaction (3).



Methyl nitrate, by analogy with the decomposition of $\text{CH}_3\text{CH}_2\text{ONO}_2$ (see, for example, ref. 49) could then undergo steps (4)-(9).



These steps are all consistent with our mass spectral results, and the reaction pattern established by Levy for ethyl nitrate.

Recently Maycock and Verneker (50) have studied the kinetics of sublimation by weight loss measurements under a stream of helium gas maintained at a pressure of 5×10^{-2} torr and found an activation energy of 109 kJ mol^{-1} .

The absence of an exotherm in their differential thermal analysis data, and the presence of decomposition products found by us strongly suggests that decomposition is preceded by sublimation and that it occurs predominantly in the vapour phase.

Fracture-induced decomposition of reactive crystals

Early work in this laboratory by Bowden, Fox and Soria-Ruiz (51, 52) had shown that when crystals of reactive materials were cleaved in vacuum then gaseous decomposition products were formed. In their initial experiments they detected the products with a quadrupole mass spectrometer, more recently we used a Bendix RCA-1A time-of-flight mass spectrometer which gave better time resolution.

Experiments on thermally very stable solids such as MgO gave no decomposition. Thermally unstable solids such as CaCO_3 (calcite) MgCO_3 and PbCO_3 produced CO_2 when cleaved. Sodium azide (non-explosive) showed some reaction. A primary explosive (lead azide) produced the equivalent of 10 monolayers of gas from its fracture surfaces and a secondary explosive (PETN) approximately 2 monolayers.

In the cases where the reactions followed relatively simple kinetics ($\text{MCO}_3 \rightarrow \text{MO} + \text{CO}_2$ for the carbonates $2\text{M}^+\text{N}_3^- \rightarrow 2\text{M}^+ + 3\text{N}_2$ for the azides) it was possible to measure the quantity of gas produced. By assuming that reaction occurred only in the crack tip region an estimate of the equivalent crack tip temperature could be made. The results are summarized in table 5,

Table 5

Material	Average No. of Monolayers Decomposed	Equivalent Crack Tip Temperature/K
Calcium carbonate	0.09	1250
Magnesium carbonate	0.37	1.5×10^4
Lead carbonate	~ 2	850
Sodium azide	0.02	1000
β -lead azide	~ 10	very large
P.E.T.N.	~ 2	kinetics too complex

The word 'temperature' in this context is used guardedly. In the first case when a crack travels at its maximum velocity there is only time for two or three oscillations of the atoms during bond rupture: this is far from an equilibrium situation. Secondly the Arrhenius equation would predict an increased amount of decomposition for either an increased temperature or changes in the activation constant or pre-exponential factor (or both).

The above result is of interest to the general question of shock initiation of explosives particularly as regards the role of rapidly compressed gas pockets. Some workers (53-55) believe that thermal effects

due to compression of interstitial gases in shock initiation experiments are not important. They do so partly on the basis of the result that the shock sensitivity of some explosives is approximately the same for both vacuum and atmospheric pressure conditions. They consider that when an explosive is placed under vacuum, there is no interstitial gas. However, this may not be true for the reason mentioned above, since it means that even when experiments are done under vacuum, the initial shock, as it fractures grains of the explosive, can produce interstitial gases. If this gas is not pumped away sufficiently quickly the resulting situation may not be very different from that when interstitial gas is present initially. Thus the observation that evacuating a granular explosive does not greatly reduce sensitivity need not mean, as early workers have argued, that the adiabatic collapse process is not important in that situation.

However, although fracture can produce gaseous products and surfaces of different reactivity we have found no evidence that fracture alone can lead to fast reaction throughout a complete sample. This has been extensively studied in this laboratory by Chaudhri (56-58) who has taken many high-speed camera sequences showing extreme fragmentation of sensitive azide crystals (lead azide and silver azide) without there necessarily being initiation. The suggestion by some workers (59-61) that the decomposition of a few neighbouring molecules or the fracture of a crystal can lead to initiation of sensitive azides does not seem tenable.

In summary then fracture alone of an explosive crystal does not lead directly to initiation. However, the fact that gases and reactive fracture surfaces are produced can mean that an explosive sample is, at least temporarily, more sensitive. This has important implications in shock or impact loading of explosives as indicated above and emphasized by Chaudhri and Field (6, 62, 63).

Fracture induced decomposition of PETN

Good quality crystals were cleaved in vacuum in the presence of the Bendix mass spectrometer. Preliminary experiments established that PETN cleaves on the (110) plane. Two types of fracture were induced (i) a low energy (slow crack) mode, in which the platform holding the crystal was slowly raised so that the crystal pressed with increasing force against a rigidly held cleaving chisel, (ii) a high energy (fast crack) mode, in which a cleaving crystal was impulsively loaded against the crystal. In both types of experiment the crystal was in a vacuum of 10^8 torr before cleavage.

The experiments showed (i) that cleavage caused decomposition; increased amounts being associated with the faster cracks, (ii) there were differences between fracture/induced decomposition and thermal decomposition and (iii) the decomposition kinetics showed differences between low and high energy fracture.

Briefly, low energy fracture gave pronounced peaks at 76 and 60 in the low mass region. As the energy put into the fracture process increased, the spectra showed an increasing proportion of 60 relative to 76. The results strongly suggest that fracture caused the detachment of a complete side chain CH_2ONO_2 ($m/e = 76$) at an early stage. If this is detached with sufficient energy it quickly degrades into small fragments ($m/e = 60$ and 16) by losing an oxygen. Evidence for oxygen was found in the low mass spectra range.

Although $m/e = 76$ appears in both thermal and fracture induced decomposition the kinetics for its formation are different. With slow thermal decomposition the PETN molecule first breaks up by failure of an oxygen - nitrogen bond producing N_2O (reaction 1 above). The $CH_2ONO_2^+ = 76$ forms after step 3 by the following ionization reaction,



In energetic fracture (and as we shall see later during another high energy situation; laser irradiation) the PETN molecule can fragment at one of the central C - C bonds with the loss of a complete side chain, followed by the loss of an oxygen atom.

With the fracture of some solids, as we have shown (91), the amount of plastic deformation (and hence heat evolved) increases with crack velocity. This heating effect is localized, but intense, and can cause decomposition. However, there are also many solids which will have a decreasing amount of plastic deformation at their crack tips as velocity increases. At high velocities the fracture is increasingly 'brittle'. Even in these solids decomposition products are likely. This is basically because rupture of bonds will cause extra vibration of the lattice with a certain probability of detachment of molecules. At low crack velocities the bond which breaks will be the weakest link in the stressed region. At the highest crack velocities bonds will have to break whatever their vibrational state; the probability of higher energies being released therefore increases. A fuller discussion of these results is in preparation.

Laser-induced decomposition of PETN

By focusing a laser pulse onto an explosive a controller 'hot-spot' is added. In these experiments PETN samples were mounted in a vacuum chamber and irradiated by Q-switched pulses from a ruby laser ($\lambda = 694.3nm$). Ionized species were produced even with the ion source of the time-of-flight spectrometer (Bendix RGA-1A) turned off. A retarding voltage of $\sim 3V$ DC prevented these species entering the ion source. Assuming all ions were single-charged and that their kinetic energy is entirely due to a thermal energy of $3eV$, an equivalent temperature of $10^4 - 10^5K$ was estimated.

With the ion repeller maintained at $3V$ DC, the minimum delay for the arrival of species was $\sim 1ms$ (the main component of this delay was the time before lasing began). For a time delay set at $1.15ms$, peaks were found at $m/e = 16(O), 18(H_2O), 28(N_2, CO), 29(HCO), 30(NO), 44(CO_2), 46(NO_2)$ etc. These were similar to the end products found in the other decomposition work. Several experiments have been made with delays in the region 1 to $\sim 5ms$ with various parts of the mass region expanded. For example at $3.3ms$ high mass peaks were observed at $m/e = 60, 76, 94, 114, 116, 128$ etc... All of these peaks were transient with the exception of the 60 and 76 peaks. At a delay of $5.6ms$ the high mass peaks were still present and low mass peaks were still detectable up to $\sim 2s$.

Since a Q-switched pulse has a duration of only $20ns$ all this indicates that partial initiation of fast reaction took place. In no case have single unconfined crystals of PETN been made to explode. However, in recent experiments with molten confined PETN explosion has been induced. A full discussion of all the PETN work is in preparation. Special techniques

and analyses were developed for handling the D.S.C. and T.G. traces so that all three parameters (actuation energy, E, frequency factor, A and order of reaction, n) could be obtained from one experiment. These are described in H.M. Hauser's thesis (64).

THERMAL DECOMPOSITION OF TETRACENE

Introduction

1 guanyl-4-nitrosoaminoguanyl tetracene, called 'tetracene'



was first prepared by Hoffmann and Roth (65). It is a solid product of the reaction between sodium nitrate and aminoguanidine in aqueous solution. It is also characterised as 1-(5' tetrazolyl)-4-guanyltetracene hydrate,



Recently crystal and molecular structure was studied by Duke (66) using an X-ray diffraction method. He found that tetracene exists in two forms, A and B, which are related polymorphs.

Tetracene is a sensitive primary explosive and is often used to sensitize other primary explosives. During the last few years tetracene has acquired considerable practical importance (67). In order to understand the mechanism by which sensitization occurs a knowledge of the physical and chemical properties of tetracene is essential. However, very little detailed investigation has been made of its various properties, and the information available in the literature is contradictory. For example, Hoffmann and Roth (65), and Patinkin et al (68) found that tetracene explodes in the solid state in the temperature range 408-418 K, however, it is reported elsewhere (69) that the material melts at 401 K. Noswitz (70) has also reported that tetracene melts below the explosion temperature. The effect of rate of heating on its explosive properties was investigated by Yoffe (71), who believes that when heated slowly in vacuum it explodes at 408 K, whereas rapid heating of the material to 445 K only causes rapid volatilization of the products, thus inhibiting an explosive build-up of the chemical reaction. Yoffe did not observe any melting. Slow thermal decomposition studies have been made by Bird et al (72) and Krien (73). Bird et al found activation energies for forms A and B of tetracene to be 148 kJ mol⁻¹ and 138 kJ mol⁻¹ respectively, which disagree with the 360 kJ mol⁻¹ found by Krien.

In this section we describe our investigations of the thermal behaviour of tetracene. A preliminary account was given at a recent conference at Mölle in Sweden (74).

Experimental

Tetracene (R.D.1357, form B) was supplied by E.R.D.E., Woolwich. Thermal analysis was performed with a Perkin-Elmer Differential Scanning Calorimeter, model DSC-2. The temperature calibration of the instrument

was done at the melting points of indium (m.p. 429.8 K) and lead (600.7 K) and the energy calibration was made with sapphire, the specific heat of which is known to five decimal places in the temperature range 0 - 1200 K. All experiments were made with argon as the purge gas at a pressure of 168 kPa. Samples to be examined were placed in aluminium foil pans supplied with the instrument. The pans were then covered with aluminium lids, and transferred to the DSC machine for various studies. In some experiments aluminium lids were tightly sealed mechanically on the pans by applying a pressure of 207 kPa with a special sealing press provided with the instrument. The samples in sealed pans are referred to as "sealed" samples and the other, in which lids are loosely placed on the pans, "unsealed" samples. Some sealed samples were prepared with argon (10^5 Pa) in the pans and these are referred to as "argon sealed" samples.

Specific heat measurements

The procedure for the specific heat measurements was similar to that described by O'Neill (75). The specific heat values of tetracene were determined in the temperature range 290-410 K. In this method a sample of known weight is heated at a constant rate of rise of temperature per second (dT/dt) and the quantity of heat per second (d) which is put into the sample to maintain this rate of rise of temperature per second measured. The specific heat is then determined using the equation

$$m c \frac{dT}{dt} = d \quad (15)$$

where m is the mass of the sample and c the specific heat. Results of a typical run are shown in figure 19. It will be seen from the traces with and without sample that the specific heat remains constant to within 4.0% throughout the temperature range, although there is a tendency towards slightly higher values at higher temperatures. In interpreting the curve care has to be taken of the contribution of any exothermic decomposition of tetracene. Our thermal decomposition studies (see figure 20) show that the contribution of decomposition up to 410 K is negligible. Table 6 shows the measured specific heat values of tetracene (16 experiments) and of sapphire, which is taken as a standard material. It will be seen that there is good agreement between our value and that obtained by Yuill (23)

Table 6 : Specific Heats of Tetracene and Sapphire

Substance	Temperature range K	Specific heats	
		Present work $J \text{ kg}^{-1} \text{ K}^{-1} \times 10^2$	Literature value $J \text{ kg}^{-1} \text{ K}^{-1} \times 10^2$
Sapphire	290 - 400	9.5 ± 0.4	9.07
Tetracene	290 - 410	15.85 ± 0.65	16.3 (Ref. 23)

The reproducibility of the instrument is 4%

Heat of reaction

When a reactive sample is heated in the DSC machine to a high enough temperature, chemical reaction (endothermic or exothermic) takes place and is registered on the DSC trace, which shows the variation of the rate of

exchange of heat per second between the sample and the machine.

By converting the temperature axis into a time axis, the area under the DSC curve divided by the weight of the sample gives the value of the enthalpy, ΔH . Samples of weight 0.2 to 2 mg were selected for this work. Moreover, samples, both sealed and unsealed, were decomposed with rate of rise of temperature in the range 0.0052 to 0.667 K s⁻¹.

When a sample was decomposed in unsealed form its DSC trace showed more than one peak, as shown in figure 20, which suggests that there are various chemical reaction schemes. For such a trace extrapolation was used in order to get the value of enthalpy corresponding to every peak. The DSC trace for sealed samples at a similar heating rate consisted of two peaks (see figure 21) at temperatures 416.5 and 442 K. On comparing the traces of the sealed and unsealed samples it becomes clear that the peak at temperature 411.5 K in the unsealed condition disappears when decomposition takes place in the sealed sample. The values of the heat of reaction for sealed and unsealed samples are shown in Table 7.

Table 7 : Heats of Reaction of Tetracene

Sample condition	Heat of Reaction J g ⁻¹			Total heat of reaction (all 3 peaks) J g ⁻¹
	1st peak	2nd peak	3rd peak	
Unsealed	270 ± 25	330 ± 40	327 ± 17	930 ± 50
Sealed	-	550 ± 40	305 ± 17	860 ± 40

The effect of rate of heating on peak temperature

Many workers (76,77,78) have shown that the peak temperature is dependent upon heating rate; this can be used to determine the activation energy for decomposition and the frequency factor. We have also found that for tetracene the peak temperature increases with heating rate; values of the heating rate used were in the range 0.0052 to 0.667 K s⁻¹. At low heating rates, for example 0.0104 K s⁻¹ (figure 22), the first peak was pronounced while the second was quite flat, and the third (not shown) very flat; in this case the temperatures of the second and the third peaks became quite sharp as the heating rate was increased (figure 23). It will be seen from figure 23 that after the first exothermic peak the DSC curve goes to the baseline (i.e. zero exothermicity) at 430 K, and we believe that the decomposition of tetracene is complete at this temperature. However, as the temperature is further increased the DSC trace shows another peak at 460 K, which we believe is due to the thermal decomposition of the produce (or products) of the decomposed tetracene. We have also found that above 478 K there is no further chemical reaction even up to 535 K. It was found that for a heating rate of 0.333 K s⁻¹ or greater the first and second peaks for the unsealed sample overlapped, as shown in figure 23, and in such a case the temperature of the first peak could not be determined. It will be seen from figure 23 that a new peak has appeared at 419 K; this peak is due to an endothermic reaction. At lower heating rates no endotherm was registered by the machine. We believe that the very small endothermic peak in the unsealed condition does not significantly influence the DSC results.

Optical microscope observations of partially decomposed tetracene showed that one of the decomposition products was a very viscous liquid of yellow colour, for both sealed and unsealed samples. The condensed phase decomposition product appears to be of a volatile nature. As with unsealed samples no residue was found after the third peak, whereas with sealed samples residue was found deposited on the walls of the container.

Peak temperatures for sealed and unsealed samples are shown in Table 8. It will be seen that the peak temperatures for various peaks for unsealed samples are slightly but consistently lower than those for the corresponding peaks for sealed samples. The small difference between the peak temperatures for air sealed samples and argon sealed samples indicates that the chemical nature of the gas surrounding the sample has a small but noticeable effect on the reaction.

Table 8 : Effect of Heating Rate on Peak Temperatures
(The temperature accuracy of machine ± 1 K)

Heating Rate $K s^{-1}$	Peak temperatures (K)							
	Unsealed sample			Sealed sample		Argon sealed sample		
	1st	2nd	3rd	2nd	3rd	2nd	3rd	
.0052	393.0	-	-	399.0	-	391.0	405.0	
.0104	397.0	401.0	-	402.5	-	397.3	416.0	
.021	402.0	405.0	421.0	407.5	420.5	403.2	428.0	
.042	406.5	410.0	431.0	411.0	429.0	407.2	436.0	
.084	411.5	415.0	440.0	416.5	442.0	410.2	441.0	
.167	417.5	421.0	450.0	422.0	452.0	-	-	
.333	-	427.0	460.0	428.0	461.0	-	-	
.667	-	432.5	-	434	-	-	-	

Kinetic Parameters

(a) Non-isothermal methods

(i) Kissinger method: As described earlier, the peak temperature is a function of heating rate. A relationship (equation 16) between peak temperature and heating rate for a first order chemical reaction has been given by Murray and White (76),

$$A e^{-E/RT_m} = \frac{E}{RT_m^2} \cdot \frac{dT}{dt} \quad (16)$$

where R is the gas constant, T the absolute temperature, $\frac{dT}{dt}$ the rate of heating, T_m the peak temperature, E the activation energy for decomposition,

and A the frequency factor. Equation (16) can be written as

$$\ln \left(\frac{\phi}{T_m^2} \right) = \ln \left(\frac{RA}{E} \right) - \frac{E}{RT_m} \quad (17)$$

where $\phi = \frac{dT}{dt}$.

Equation (17) shows that a graph between $\ln \left(\frac{\phi}{T_m^2} \right)$ and $\frac{1}{T_m}$ is a straight line of slope $-E/R$. Kissinger (77) found that for the decomposition of clays the graph between $\ln \left(\frac{\phi}{T_m^2} \right)$ and $\frac{1}{T_m}$ was a straight line, and found E from the slope. Knowing the value of E, A can be determined using equation (16).

For an n^{th} order reaction a relationship between ϕ and T_m is given by equation (18) (see Kissinger, 79):

$$\frac{E\phi}{RT_m^2} = A n (1-x)_m^{n-1} e^{-E/RT_m} \quad (18)$$

in which $(1-x)_m$ is the fraction of the material unreacted at the peak temperature T_m . Kissinger has shown that the product $n(1-x)_m^{n-1}$ is not only independent of ϕ , but is very nearly equal to unity. Therefore equation (18) reduces to equation (16). Hence the Kissinger method is applicable regardless of the order of the reaction.

Plots of $\ln(\phi/T_m^2)$ vs. $\frac{1}{T_m}$ for tetracene are shown in figures 24 and 25. The values of the activation energies and the frequency factor corresponding to various peaks are shown in Table 9. It is interesting to note that the activation energies for decomposition corresponding to the first and third peaks are slightly different for sealed and unsealed samples. Argon also appears to have a small effect on the decomposition parameters.

(ii) Ozawa method: A method which is slightly different from that of Kissinger has been developed by Ozawa (78), who showed that the graph of $\ln \phi$ vs. $\frac{1}{T_m}$ is a straight line of slope $-0.457 E/R$. This method was originally used for analyzing thermogravimetric data but has also been successfully used by Krien (80) for the analysis of DSC data.

We have also applied this method to our DSC data and found that the graph of $\ln \phi$ vs. $\frac{1}{T_m}$ is a straight line as shown in figures 25 and 26. The values of activation energies for the decomposition of tetracene found using this method are included in Table 9, and they agree well with the values found using the Kissinger method.

Table 9 : Activation Energies, $E(\text{kJmol}^{-1})$ and Frequency Factor, $A(\text{s}^{-1})$, using Kissinger and Ozawa Methods.

Kissinger Method						
Sample condition	1st peak		2nd peak		3rd peak	
	E	log A	E	log A	E	log A
Unsealed	193 ± 6	22.6	177 ± 2	20.3	109 ± 11	10.7
Sealed	-	-	192 ± 5	22.1	98 ± 6	9.3
Argon sealed	-	-	210 ± 20	24.5	110 ± 14	10.7

Ozawa Method			
Sample condition	1st peak	2nd peak	3rd peak
	E	E	E
Unsealed	200 ± 6	184 ± 2	122 ± 15
Sealed	-	190 ± 6	105 ± 6
Argon sealed	-	215 ± 17	118 ± 9

(b) Isothermal methods:

We have used two isothermal methods for the determination of activation energy for thermal decomposition.

(i) Slow thermal decomposition: A small amount (100-300 μg) of tetracene was sealed in a pan as described earlier; the pan was then placed in the sample holder of the DSC machine heated to 330 K. Immediately after this the temperature of the sample holder was raised at a high heating rate of 5.33 K s⁻¹, to a chosen temperature and then kept constant at this temperature till the sample decomposed completely. A typical DSC trace at constant temperature is shown in figure 28. From this trace the amount of fractional decomposition, α , at any time, t , can be obtained by dividing the area under the curve up to t by the total area under the curve. It is to be noted that we have assumed that the sample decomposes completely when the DSC trace comes back to the baseline. Our powder X-ray work has confirmed this. As described earlier, we have also assumed that the third peak is only due to the decomposition of the product of decomposed tetracene, and since the third peak is well separated from the first and second peaks for the unsealed sample or the second peak for the sealed sample, no contribution is made by the decomposition of the product (i.e. corresponding to the third peak) to the area under the curve corresponding to the decomposition of tetracene.

DSC traces for various chosen temperatures were obtained and the data α -t curves in figure 29; these α -t curves are of the well-known (81-84) 'sigmoid shape'. An Arrhenius plot for the acceleratory period is shown in figure 30, which is a straight line from which the value of the activation energy for decomposition obtained is $201 \pm 3 \text{ kJ mol}^{-1}$. There is good agreement between this value and the values corresponding to the second peak of the sealed sample obtained by the Kissinger and Ozawa methods.

(ii) Ignition time: When a reactive material is suddenly raised to a high enough temperature it ignites after a time delay, t_{exp} . Many investigators (34,60,85,86) have found that for various materials a relationship of the type shown in equation (19) exists between t_{exp} , E and T :

$$\ln t_{\text{exp}} = B + E/RT \quad (19)$$

where B is a constant.

We have used the DSC machine to find the values of t_{exp} at various temperatures for small unsealed samples of tetracene. The experimental procedure was as follows:

An unsealed tetracene sample was placed in the DSC holder and heated to 330 K, and then the temperature of the machine raised rapidly at a rate of 5.33 K s^{-1} to a chosen temperature. After a delay time, t_{exp} , ignition of the sample occurred; t_{exp} down to $\frac{1}{2}$ s was measured on a chart recorder and a graph of $\ln t_{\text{exp}}$ and $1/T$ is shown in figure 31, which is a straight line. The value of E obtained from this graph is $195 \pm 17 \text{ kJmol}^{-1}$ which is again in good agreement with all the methods described above.

Discussion

This DSC investigation has shown that the decomposition of tetracene is a complex process. As the temperature of an unsealed sample is raised we may see an endothermic peak which corresponds with sublimation or dehydration of tetracene (see figure 23); this endothermic peak only appears at higher heating rates. At lower heating rates the peak is so spread out that its magnitude becomes negligible on the trace. In another series of experiments we have investigated mass-spectrometrically the products evolved as the temperature of tetracene was raised to the values when decomposition started. We found that at temperatures corresponding to the endothermic peak some water was evolved. On the basis of these observations we believe that the endothermic peak corresponds with some dehydration of tetracene and not sublimation as has been suggested by Norwitz (70).

When the temperature of the sample is above the temperature corresponding to the endothermic peak, exothermic reaction starts to occur, and an examination of the product of decomposition with an optical microscope during the first peak, revealed the existence of a very viscous liquid phase in the sample. It has been suggested by some workers (69,70) that tetracene melts at temperatures very close to its explosion temperature. We have taken cine camera photographs (32 frames s^{-1}) at a magnification of x80 of powder samples of tetracene being heated up to the explosion temperature. In all eleven experiments were made, and in two of them formation of small globules were observed just before explosion. We are not certain whether the globules were of molten tetracene or liquid

products of decomposition. Our X-ray analysis of the residue after the first two peaks has shown that along with the liquid product, solid decomposition products are also formed. At present we do not know what these products are.

These products themselves decompose exothermically at higher temperatures and produce the 3rd peak. Their decomposition products appear to sublime. It is these volatile products which can deposit on sensitive instruments incorporated in the vacuum system in which decomposition is studied. On account of this, decomposition studies of tetracene in vacuum are not suitable and the DSC has an advantage over the pressure-time method.

We have used four different methods to calculate the activation energy for decomposition. All the methods gave values which agreed with one another. Attempts to obtain the activation energy using Roger and Morris's (87) method were not successful, as the value found by this method was very different from the values obtained by the other methods. The Roger and Morris method is applicable only to zero order decomposition reaction, which is not the case for the decomposition of tetracene.

We have found that the α -t curve can be described by an Avrami-Erofeev equation

$$[-\ln(1-\alpha)]^{1/6} = kt \quad (20)$$

Figure 32 shows a comparison between experiment and theory (equation 20). The experimental curve includes data for all the temperatures studied. The agreement is good for $\alpha = 0.1$ to $\alpha = 0.90$. The discrepancy for $\alpha < 0.1$ may be due to the difficulty in establishing zero time from the DSC traces. Such a difficulty has been responsible for the lack of agreement in the theory and experiment in some other work on decomposition (88). The value of the activation energy obtained by using equation (20) is 198 kJmol^{-1} , which is in good agreement with the experimentally determined values. The value of $n = 6$ in equation (20) suggests that the reaction follows a power nucleation law with nuclei growing three dimensionally.

Since the decomposition products of tetracene also decompose exothermically (see figures 20,21), care has to be taken in calculating the heat of reaction. X-ray powder photographs of the residue after the end of the second peak showed that the original tetracene sample had decomposed completely. This means that the true heat of reaction of tetracene should be calculated for the first 2 peaks. However, in conditions of fast reaction total heat of reaction must include the 3rd peak as well. Our values are appreciably smaller than the 1192 J g^{-1} obtained by Krien (73), and the 2270 J g^{-1} (for explosion) reported elsewhere (89, 90).

References

1. Tabor D., Field J.E., Chaudhri M.M., Winter R.E., Ng W.L. and Heavens S.N. 1974, Final Report, Contract No. DAJA-37-73-C-4059.
2. Heavens S.N. and Field J.E. 1974, Proc. Roy. Soc. A338, 77.
3. Andreev K.K., Maurina N.D. and Rusakova Yu.A. 1955, Dokl. Akad. Nauk SSSR 105, 533.
4. Ljungberg S. 1958, Nobel Hefte 24, 40.
5. Schroeder W. and Webster D.A. 1949, J. Appl. Mech. 16, 289.
6. Chaudhri M.M. and Field J.E. 1977, Chapter in "Properties of the Azides" (Ed. R. Walker) Plenum Press, 1977.
7. Afanas'ev G.T. and Bobolev V.K. 1971, Initiation of Solid Explosives by Impact. Transl., Israel Program for Scientific Transl., Jerusalem.
8. Kholevo N.A. 1946, Tr. Kazansk. Khim. Tech. Inst. 10, 91; *ibid.* 1947, 11, 116.
9. Plant J. 1972, Phys. Bull. 23, 203.
10. Belajev A.F. and Chariton J.B. 1936, Acta Phys-Chim. URSS, 5, 757.
11. Courtney-Pratt J.A. and Rogers G.T. 1953, Nature 175, 176.
12. Winter R.E. and Field J.E. 1975, Proc. Roy. Soc. A343, 399.
13. Shelton H., Hendricks C.D. and Weurker R.F. 1960, J. Appl. Phys. 31, 1243.
14. Winter R.E. 1971, PhD thesis, University of Cambridge.
15. Zener C. and Hollomon H.J. 1944, J. Appl. Phys. 15, 22.
16. Recht R.F. 1964, J. Appl. Mech. 31, 189.
17. Stock T.A.C. and Thomson K.R.L. 1970, Metall. Trans. 1, 219.
18. Afanas'ev G.T., Bobolev V.K., Kazarova Yu.A. and Karabanov Yu.F. 1972, Fiz. Goreniya i Vzryva 8(2), 299.
19. McKenzie D. and Brune J.N. 1972, Geophys. J.R. Astr. Soc. 29, 65.
20. Andrianova G.P., Kechekyan A.S. and Kargin V.A. 1971, J. Polymer Sci. A-2, 9, 1919.
21. Roseen R. 1974, J. Mat. Sci. 9, 929.
22. Winter R.E. 1975, Phil. Mag. 31, 765.
23. Yuill A.M. 1953, PhD Thesis, University of Cambridge.
24. Blackburn J.H. and Seely L.B. 1965, Trans. Farad. Soc. 61, 537.
25. Rideal E.K. and Robertson A.J.B. 1949, Proc. Roy. Soc. A195, 135.
26. Bowden F.P. and Tabor D. 1954, "The Friction and Lubrication of Solids" Pt. I, O.U.P. 1954; "The Friction and Lubrication of Solids", Pt. II, O.U.P. 1964.
27. Highway R.J. and Taylor D.S. 1966, Wear 9, 310.
28. Bowden F.P., Stone M.A. and Tudor G.K. 1947, Proc. Roy. Soc. A188, 329.
29. Hill R. 1950 "The Mathematical Theory of Plasticity" p.215 (O.U.P.)
30. Blok H. 1937, Inst. Mech. Engrs. 2, 222.
31. Amuzu J.K.A., Briscoe B.J. and Chaudhri M.M. 1976, J. Phys. D. 9, 133.
32. Chaudhri M.M. 1976, Nature 263, 121.

33. Bowden F.P. and Yoffe A.D. 1952, Initiation and Growth of Explosion in Liquids and Solids, C.U.P.; and 1958, Fast Reactions in Solids, Butterworth, London.
34. Tabor D. 1972, Surface and Colloid Science, Vol. 5 ed. E. Matijevic, Wiley, London, p.245; and 1974, Advances in Polymer Friction and Wear, Vol. 5A, ed. L. Lee, Plenum, London, p.5.
35. Bowden F.P. and Tabor D. 1943, J. Appl. Phys. 14, 141.
36. Bowden F.P. and Tabor D. 1966, Br. J. Appl. Phys. 17, 1521.
37. Timoshenko S. and Goodier J.N. 1951, Theory of Elasticity, McGraw-Hill, New York.
38. Greenwood J.A. and Williamson J.B.P. 1966, Proc. Roy. Soc. A295, 300.
39. Archard J.F. 1974, Tribology International, 213.
40. Tabor D. 1975, Wear 32, 269.
41. Tabor D. 1970, Rev. Phys. Technol. 1, 145.
42. Swain M.V. and Lawn B.R. 1969, Phys. Stat. Solidi 35, 909.
43. Briscoe B.J., Scruton B. and Willis R.F. 1973, Proc. Roy. Soc. A333, 99.
44. Amuzu J.K.A., Briscoe B.J. and Tabor D. 1977, Trans. A.S.L.E., April. and 1976, Proc. Japan. Soc. Lubrication Engrs. Conf. Tokyo 1975, Elsevier Scientific Pub. Co. p.155.
45. Briscoe B.J. and Tabor D. 1974, Trans. A.S.L.E. 17, 158; and 1975, Wear 34, 29.
46. Baier R.E. and Zisman W.A. 1970, Macromolecules, 3, 262.
47. Ng W.L., Field J.E. and Hauser H.M. 1976, J. Chem. Soc. Perkin trans. II, p.637.
48. Levy J.B. 1954, J. Am. Chem. Soc. 76, 3790.
49. Benson S.W. 1960 "The Foundations of Chemical Kinetics", McGraw-Hill Book Co., New York.
50. Maycock J.N. and Pai Verneker V.R. 1970, Thermochemica Acta 1, 191.
51. Bowden F.P., Fox P.G. and Soria-Ruiz J. 1968, Nature 220, 778.
52. Bowden F.P. and Gurton O.A. 1949, Proc. Roy. Soc. A198, 337.
53. Cachia G.P. and Whitbread E.G. 1958, Proc. Roy. Soc. A246, 268.
54. Campbell A.W., Davis W.C. and Travis J.R. 1961, Phys. Fluids 4, 498.
55. Chick M.S. 1965, Proc. 4th Int. Symp. on Detonation, O.N.R., p.349.
56. Chaudhri M.M. 1969, PhD Thesis, Cambridge University.
57. Chaudhri M.M. and Field J.E. 1970, Proc. 5th Int. Symp. on Detonation, O.N.R., p.301.
58. Chaudhri M.M. 1972, Combustion and Flame 19, 419.
59. Taylor W. and Weale A. 1932, Proc. Roy. Soc. A138, 92.
60. Ubbelohde A.R. 1948, Phil. Trans. A241, 199.
61. Fox P.G. 1970, J. Solid State Chem. 2, 491.
62. Chaudhri M.M. and Field J.E. 1974, Proc. Roy. Soc. A340, 113.
63. Field J.E. 1975, Plenary Lecture, Proc. Int. Conf. on Primary Explosives, E.R.D.E. Waltham Abbey, U.K.

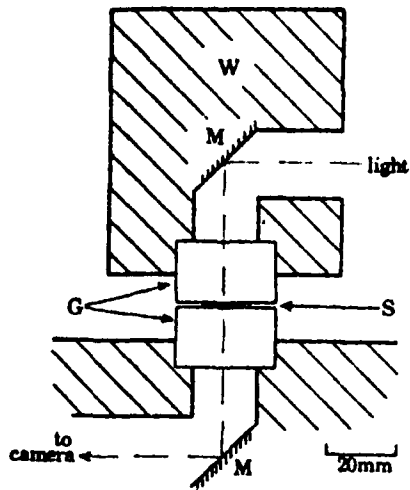
64. Hauser H.M. 1977, PhD Thesis, Cambridge University.
65. Hoffman K.A. and Roth R. 1910, Ber. 43, 682.
66. Duke J.R.C. 1971, Chem. Commun. 2.
67. Taylor G.W.C., Holloway K.J., Thomas A.T. 1965, British Patent 985, 293, March 3.
68. Patinkin S.H., Horwitz J.P. and Liebev E. 1955, J. Amer. Chem. Soc. 77, 562.
69. Military Specification MIL-I-46938 A(MU), Tetracene, 5 April 1971.
70. Norwitz G., Everett M.E. and Curbarc M.T. 1974, AD/A-005163, National Technical Information Service, U.S.
71. Yoffe A.D. 1951, Proc. Roy. Soc. 208, 188.
72. Bird R., May F.G.J. and Warren M.D. 1975, 5th Quadripartite Ammunition Conference, Canberra.
73. Krien G. 1970, 2nd Symp. on Chemical Problems connected with the Stability of Explosives, Tyringe, Swedish Combustion Institute, p.102.
74. Patel R.G. and Chaudhri M.M. 1976, Proc. 4th Symp. on Chemical Problems associated with the Stability of Explosives, Mölle, Sweden.
75. O'Neill M.J. 1966, Anal. Chem. 38, 1331.
76. Murray P. and White J. 1955, Trans. Brit. Ceram. Soc. 54, 204.
77. Kissinger H.E. 1956, J. Research Nat. Bur. Standards 57, 217.
78. Ozawa Z. 1965, Bull. Chem. Soc. Japan 38, 1881.
79. Kissinger H.E. 1957, Anal. Chem. 29, 1702.
80. Krien G. 1973, 3rd Symposium on Chemical Problems Connected with the Stability of Explosives, ed. J. Hansson, Ystad, May.
81. Young D.A. 1966, "Decomposition of Solids" Pergamon, Oxford, p.2.
82. Garner W.E. and Halies H.R. 1933, Proc. Roy. Soc. A139, 576.
83. Garner W.E. 1955, Chem. of Solid State, ed. Garner W.E., Butterworths Scientific Publication, p.232.
84. Wee-lam Ng 1975, Aust. J. Chem. 28, 1169.
85. Sinha S.K., Shrivastva R.C. and Surve R.N. 1975, Conf. on Primary Explosives E.R.D.E.
86. Fine D.H. and Gray P. 1967, Combustion and Flame 11, 71.
87. Roger R.N. & Morris E.D. 1957, Anal. Chem. 38, 41.
88. Galway A.K. and Jacob P.W.M. 1960, Proc. Roy. Soc. A254, 455.
89. AMC Pamphlet 706-177, March 1967, US Army Material Command, USA.
90. Urbanski T. 1964, Chemie und Tech. der Explosivstoffe, Leipzig, Band III, S180.
91. Fuller K.N.G., Fox P.G. and Field J.E. 1975, Proc. Roy. Soc. A341, 537.
92. Wilson M.P.W. 1967, PhD Thesis, University of Cambridge.

Figure Captions

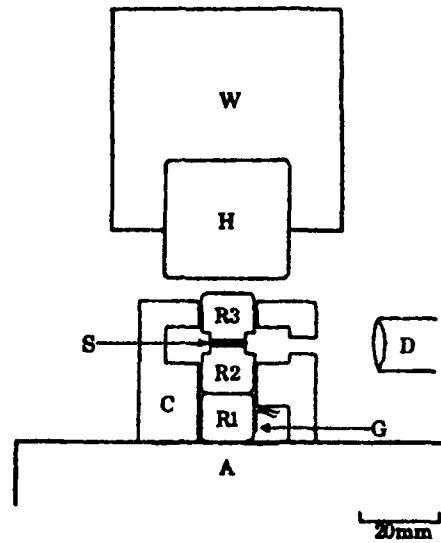
1. Experimental arrangement at instant of impact. W - drop-weight; G - glass blocks; M - mirrors; S - sample. The upper glass block G is attached to the drop-weight.
2. Impact of a layer of granular PETN viewed in transmitted light. The sample flows plastically, melts and ignites at a number of sites. The thickness of the layer at the time of ignition is about 50 μm . In frames 8 and 9, D is a flaw in the glass surface and I is an ignition site. Mass of sample 14 mg. Diameter of field of view 20 mm. Interframe time 5.5 μs .
3. Experimental arrangement for obtaining pressure-time curves. W - drop-weight; H, R1, R2, R3 - hard rollers; C - cylindrical guiding sleeve; S - sample; G - strain gauge; A - cast steel anvil; D - light detector.
4. Pressure-time curves for impact of RDX. Similar behaviour is shown by PETN, HMX, and ammonium perchlorate. Mass of hammer 5 kg. Drop-height (a) 0.35 m (b) 0.2 m (c) 0.5 m (d) 0.25 m. Horizontal scale 100 μs /division. Vertical scale 5 mV/division (4.3 kbar/division). The instant of ignition is recorded by the beginning of the light detector pulse in (a), (b) and (c) and by the electrical short-circuit in (d).
5. Radius of a layer of PETN during impact, showing evidence of plastic flow followed by jetting, melting and ignition.
6. Velocities versus particle size for iron and silver spheres accelerated by electrostatic method. Charging surface at $5 \times 10^8 \text{ Vm}^{-1}$, accelerating potential 80 kV. See Shelton et al (13), Winter (14) for details of method.
7. The explosive driver technique used to accelerate particles in the range 50 - 500 μm .
8. The method of mounting the silver azide crystals.
9. A plastic indentation produced by the impact of an 80 μm aluminium sphere on a polished silver azide crystal at a velocity of 200 m s^{-1} .
10. (a) Part of a vertical section through an indentation produced in titanium by the impact of a 4 mm steel sphere at 385 m s^{-1} . The dark lines intersecting the crater surface obliquely are adiabatic shear bands; one is shown at a higher magnification in (b).
11. The general positions of shear bands observed by Stock and Thomson (17) and Wilson (22), in metal targets impacted by projectiles with spherical tips. The figure also provides a model for calculating the temperatures produced on these bands.
12. Situations in which shear concentrations could occur when an explosive consisting of small crystals pressed together (a 'compact') is impacted.

13. Adhesion of particles to the indenter tip during penetration.
14. Calculated temperature rise against indenter penetration graphs when two conical indenters of different masses but having the same initial kinetic energy impact a column of compacted lead azide. a) indenter mass 0.145 kg, velocity 0.5 m s^{-1} ; b) indenter mass 0.290 kg, velocity 0.353 m s^{-1} . Both indenters come to rest at a penetration of 1.16 mm. Note that the steady-state temperatures are reached well before the indenters come to rest.
15. Schematic diagram of the sliding configurations and apparatus: (a) single crystal on single crystal; (b) single crystal on glass; (c) thin film between glass surfaces; (d) apparatus with normal load W and frictional force F . The magnifications of the contacts are greatly expanded in the vertical direction.
16. Coefficient of friction as a function of load. Configuration (a): PETN (on PETN), \ominus . Configuration (b): HMX, \ominus ; RDX, \ominus ; PETN, \ominus ; AgN_3 , \ominus ; $\text{Pb}(\text{N}_3)_2$, \ominus . Sliding speed 0.2 mm s^{-1} , temperature 20°C .
17. Shear strength τ as a function of contact pressure P . Configuration (c): $\text{Pb}(\text{N}_3)_2$, \ominus ; AgN_3 , \ominus ; PETN, \ominus . Sliding speed 0.2 mm s^{-1} , temperature 20°C .
18. Temperature dependence of the shear strength τ and the hardness H_V plotted as $\lg \tau$ and $\lg H_V$ against the reciprocal of temperature. Shear strength experiments: contact pressure, $6.7 \times 10^7 \text{ Pa}$; sliding speed 0.2 mm s^{-1} . AgN_3 , \ominus ; PETN, \ominus . Hardness experiments: load 0.15 N; loading time 60 s. PETN, ∇ .
19. DSC trace for the measurement of specific heat of tetracene.
20. DSC trace for unsealed sample of tetracene at a heating rate of 0.084 K s^{-1} .
21. DSC trace for sealed sample of tetracene at a heating rate of 0.084 K s^{-1} .
22. DSC trace for unsealed sample at a heating rate of 0.0104 K s^{-1} . Only first two peaks are shown. Note that peaks are much spread out as compared with those in figures 20, 21 and 23.
23. DSC trace for unsealed sample. Heating rate 0.333 K s^{-1} . An endothermic peak appears at 419 K.
24. Plots of $\ln(\phi/T_m^2)$ vs. $1/T_m$ for first and second peaks under various conditions. Unsealed sample: Δ - first peak, \bullet - second peak; Sealed sample: \circ - second peak; Argon sealed sample: \blacktriangle - second peak.
25. Plots of $\ln\phi$ vs. $1/T_m$ for first and second peak under various conditions. Unsealed sample: Δ - first peak, \bullet - second peak; Sealed sample: \circ - second peak; Argon sealed sample: \blacktriangle - second peak.
26. Plots of $\ln\phi$ vs. $1/T_m$ for third peak under various conditions. \bullet - unsealed sample, \circ - sealed sample, \blacktriangle - Argon sealed sample.

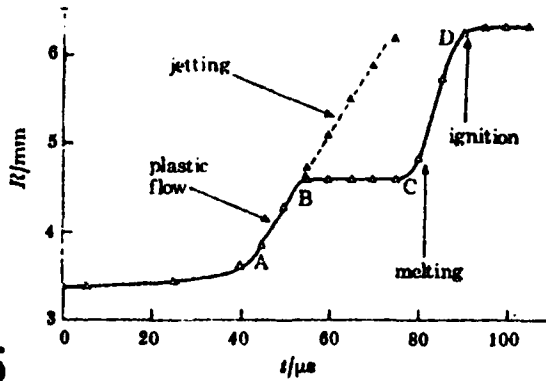
27. Plots of $\ln(\phi/T_m^2)$ vs. $1/T_m$ for third peak under various conditions.
● - Unsealed sample, ○ - Sealed sample, ▲ - Argon sealed sample.
28. DSC trace for decomposition of tetracene at temperature 412 K.
29. α -t curves of decomposition of tetracene at various temperatures.
○ - 396 K, ● - 400 K, ⊖ - 403 K, Δ - 405 K, □ - 408 K, ⊙ - 412 K.
30. Arrhenius plot for the acceleratory period.
31. Plot of explosion delay time vs. reciprocal of absolute temperature.
32. Comparison between experiments and equation (20). $t_{0.5}$ represents time for 50% decomposition at any isothermal temperature. ▲ - 396 K, □ - 400 K, Δ - 405 K, ● - 408 K, ○ - 412 K, ----- exp., ——— theory.



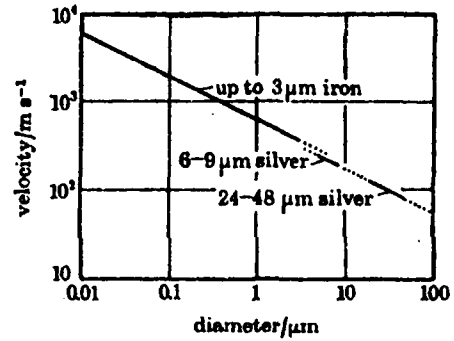
1



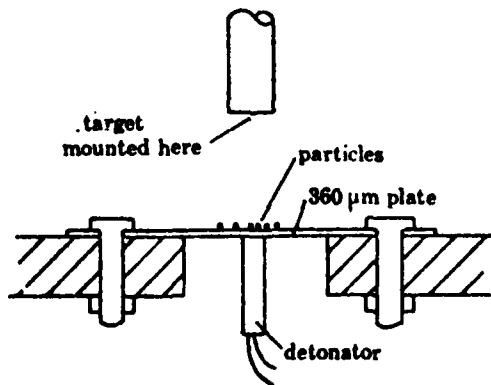
3



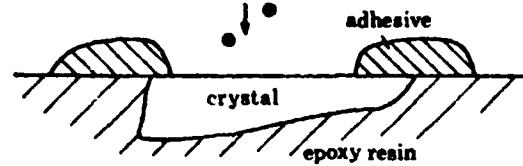
5



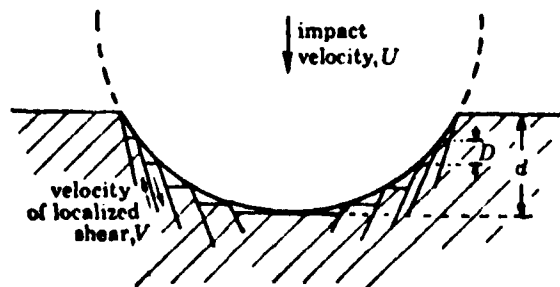
6



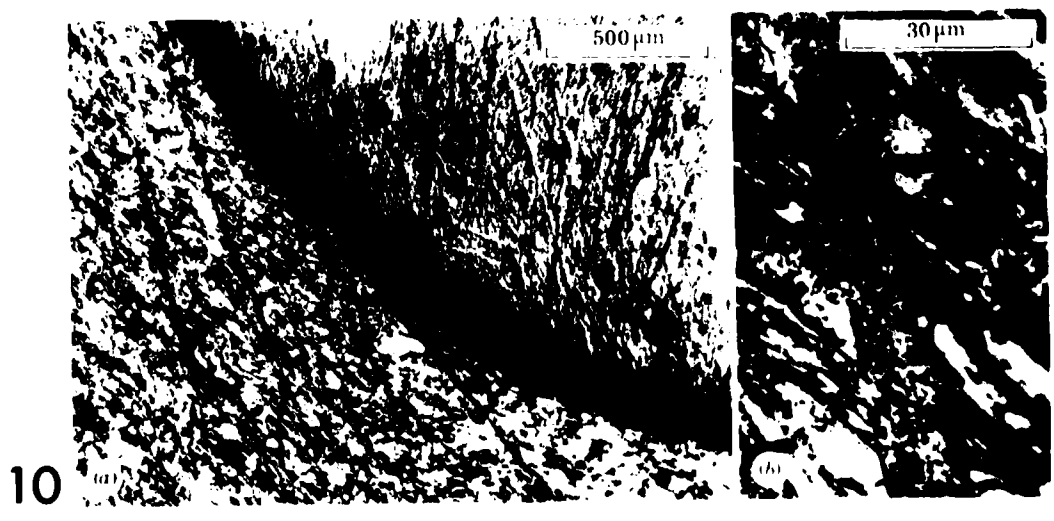
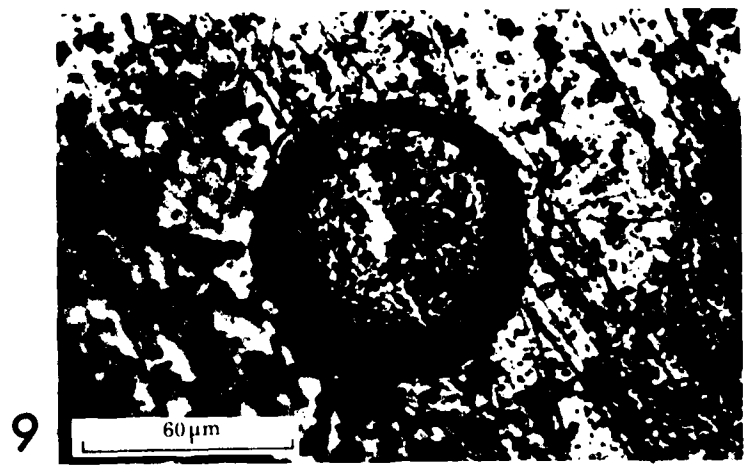
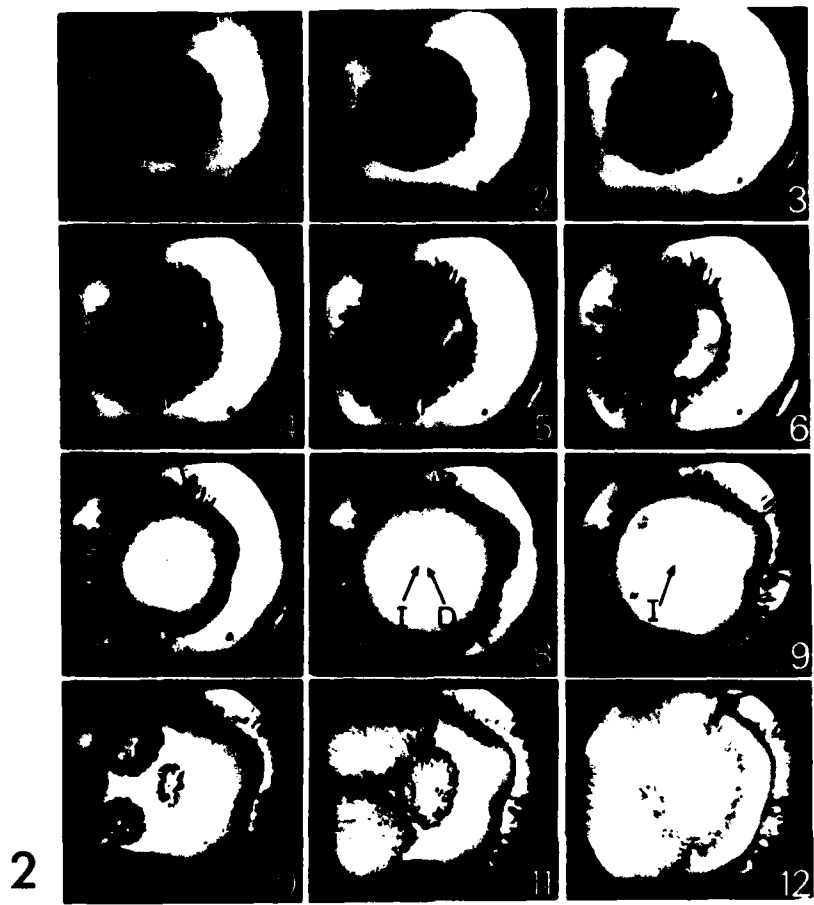
7



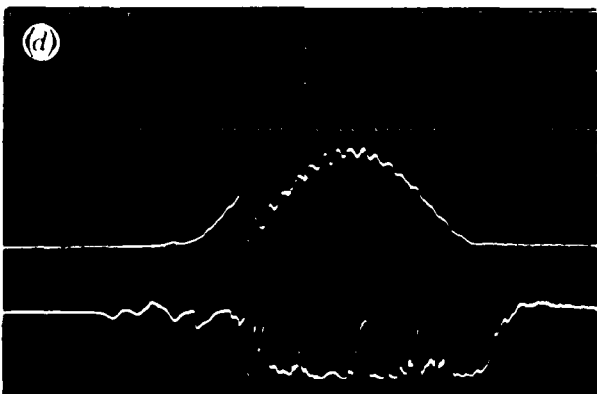
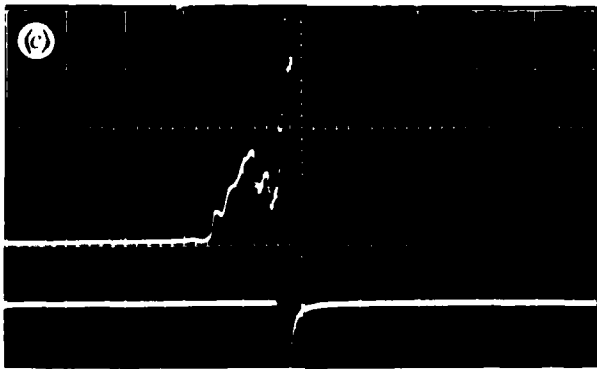
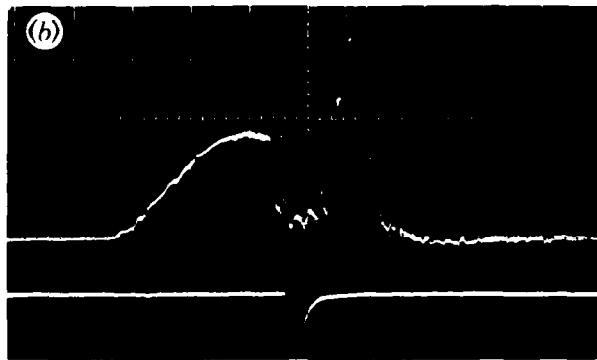
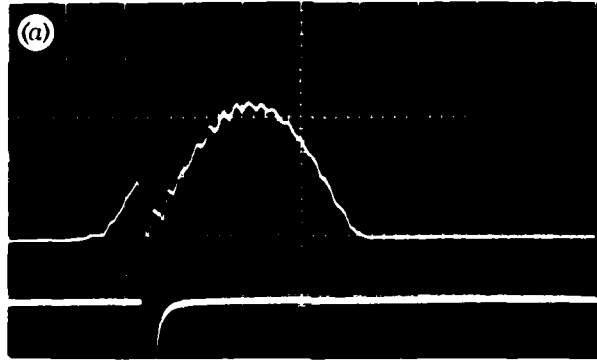
8

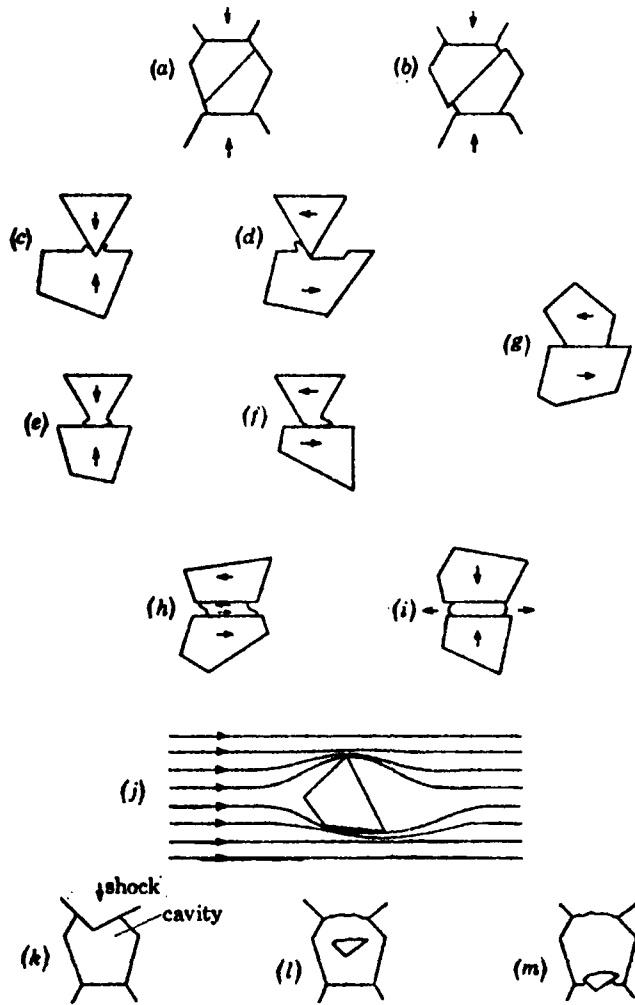


11

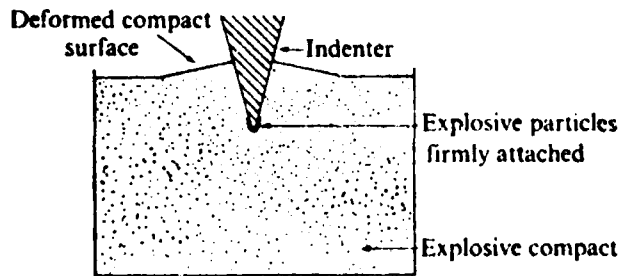


4

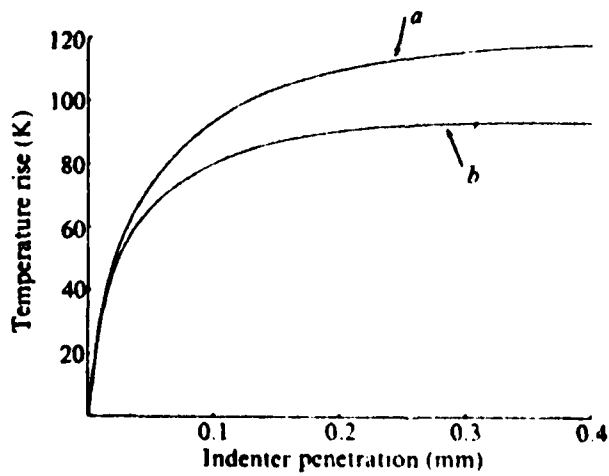




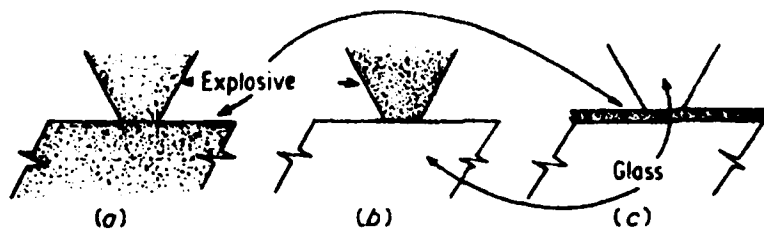
12



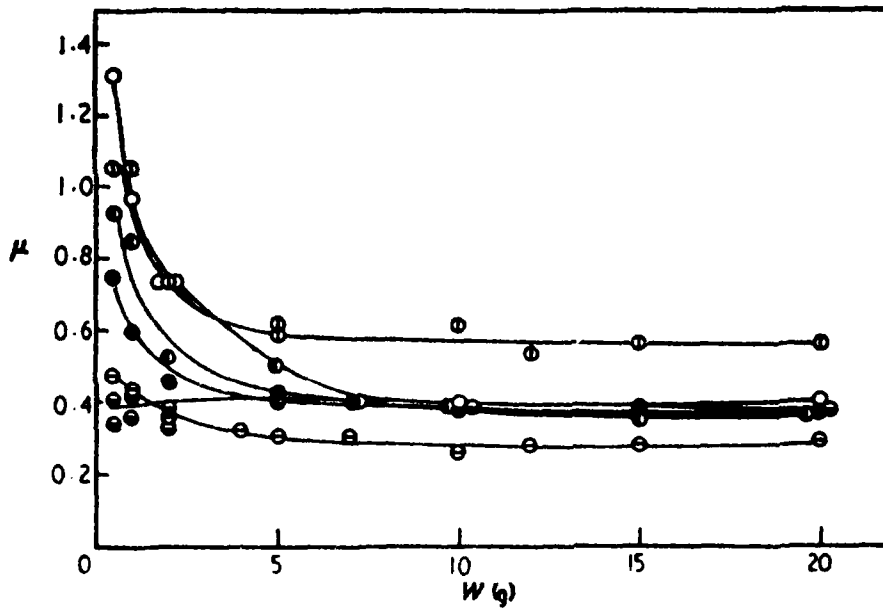
13



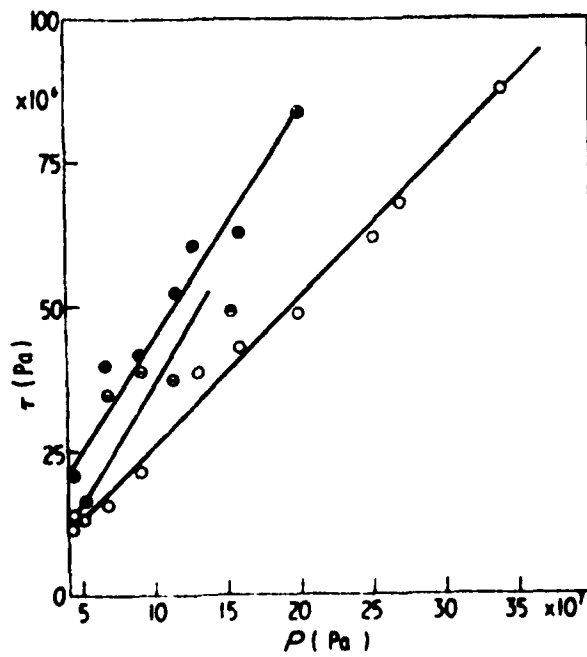
14



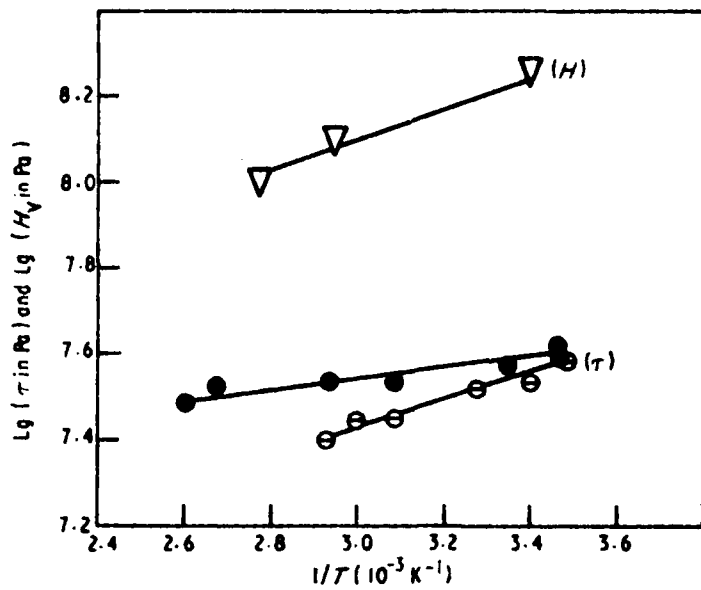
15



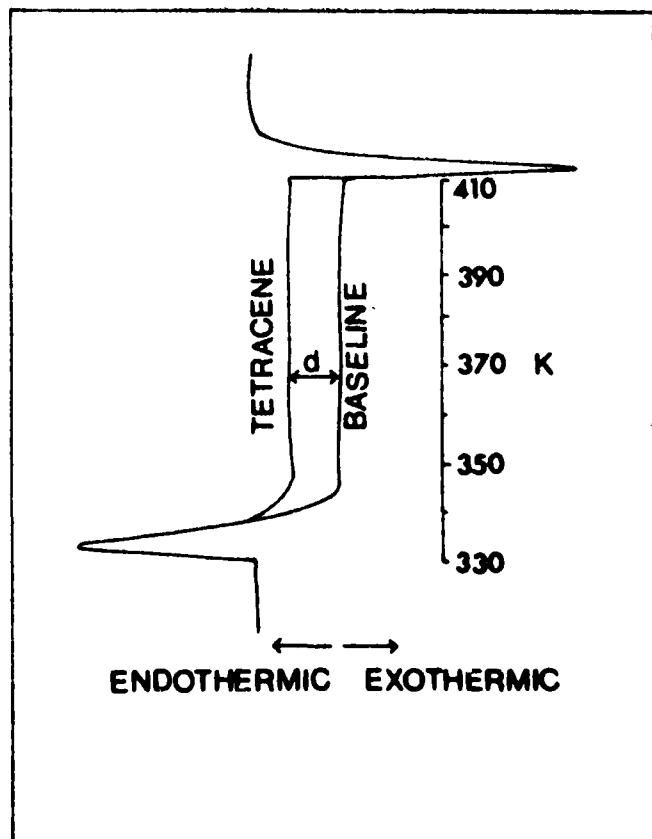
16



17

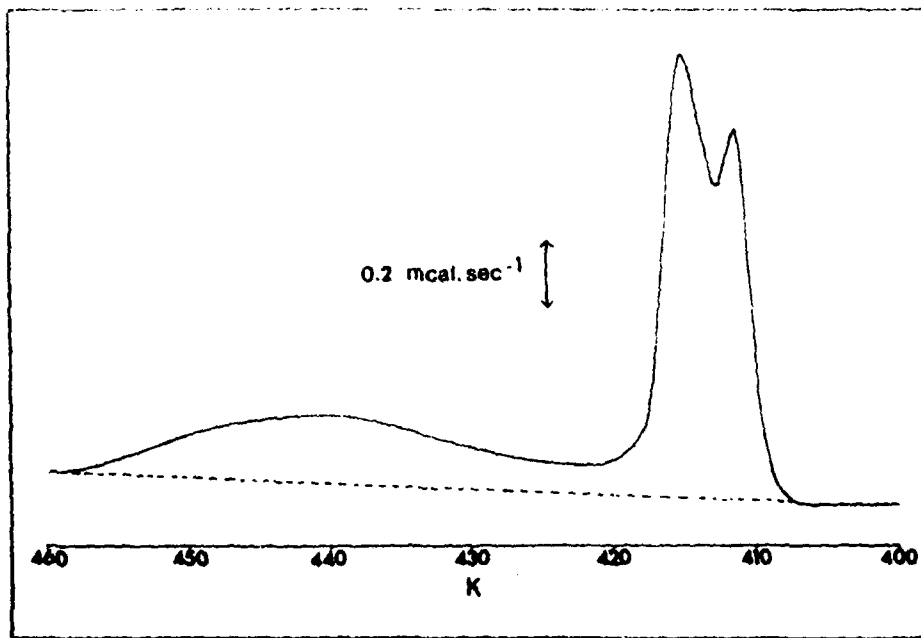


18

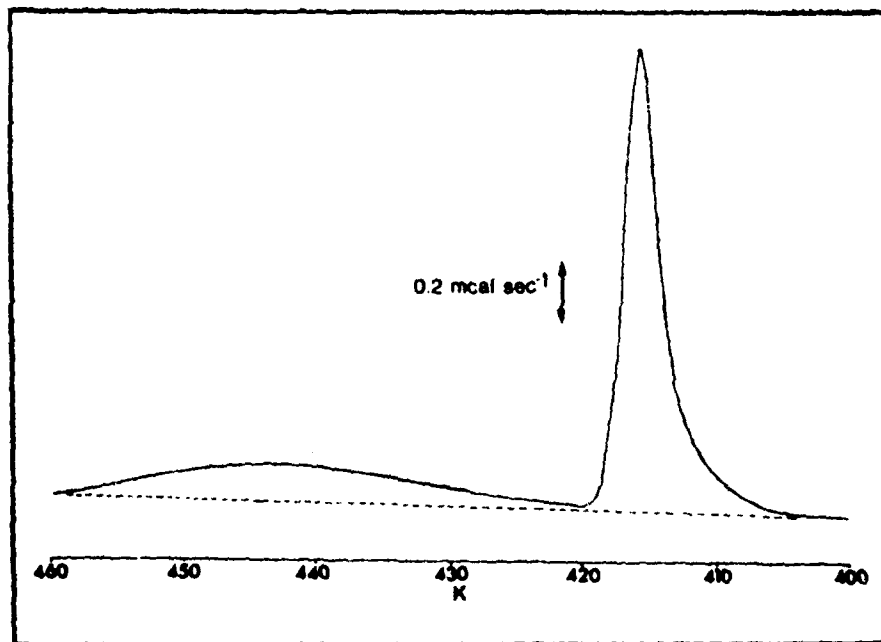


19

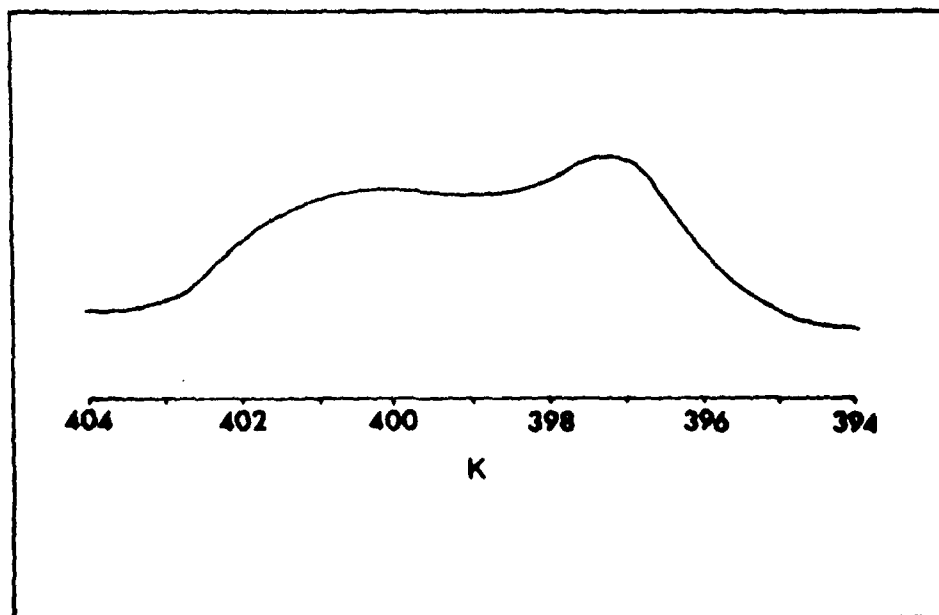
20



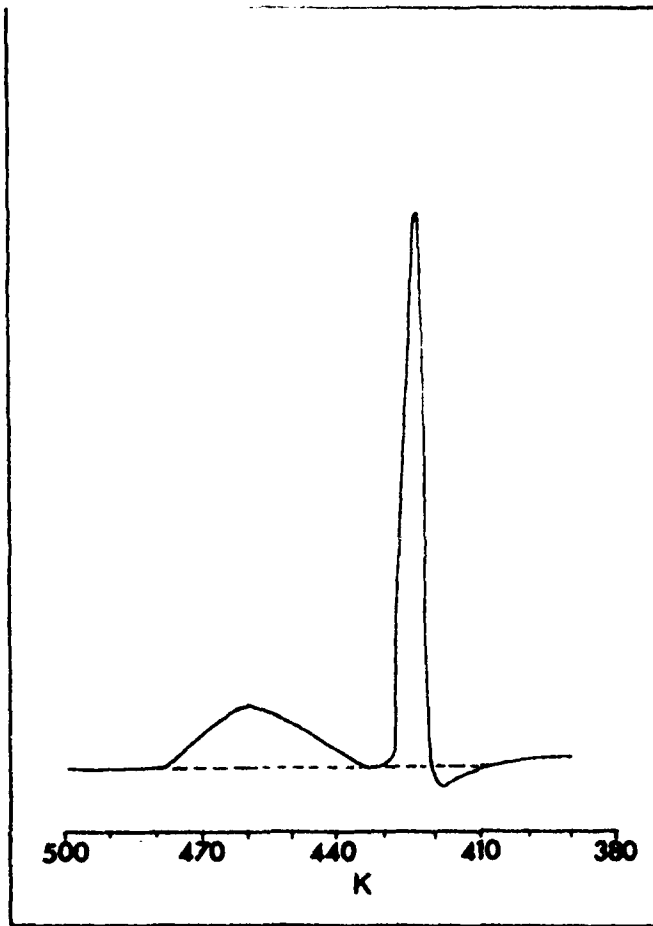
21



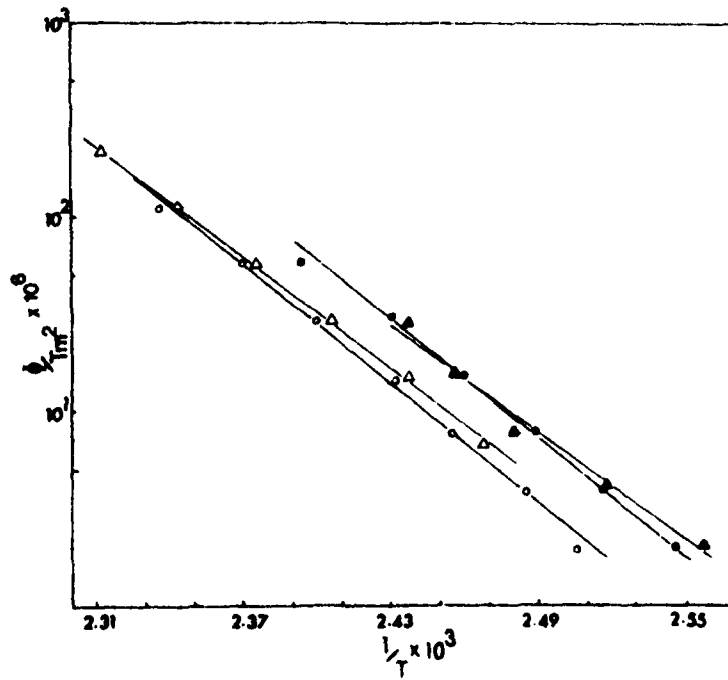
22



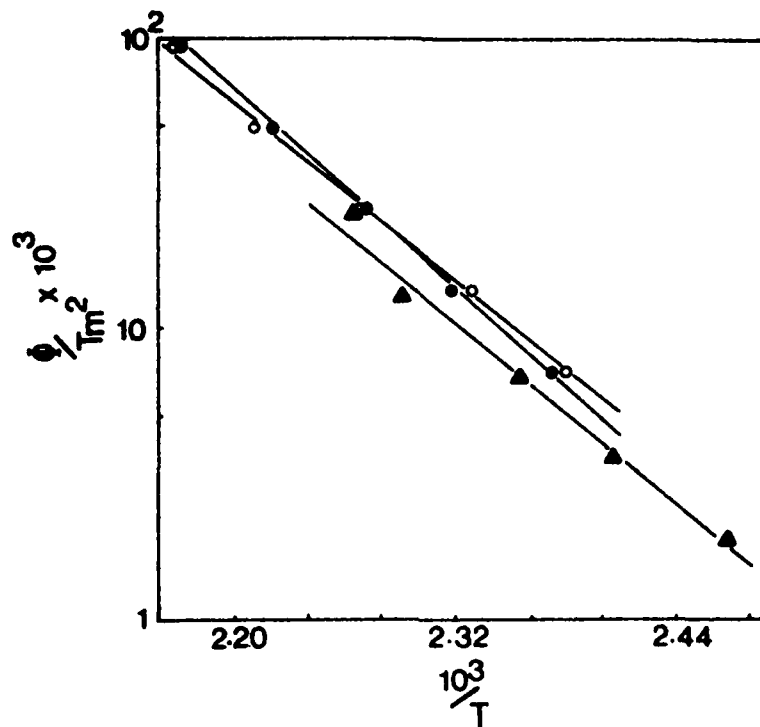
23



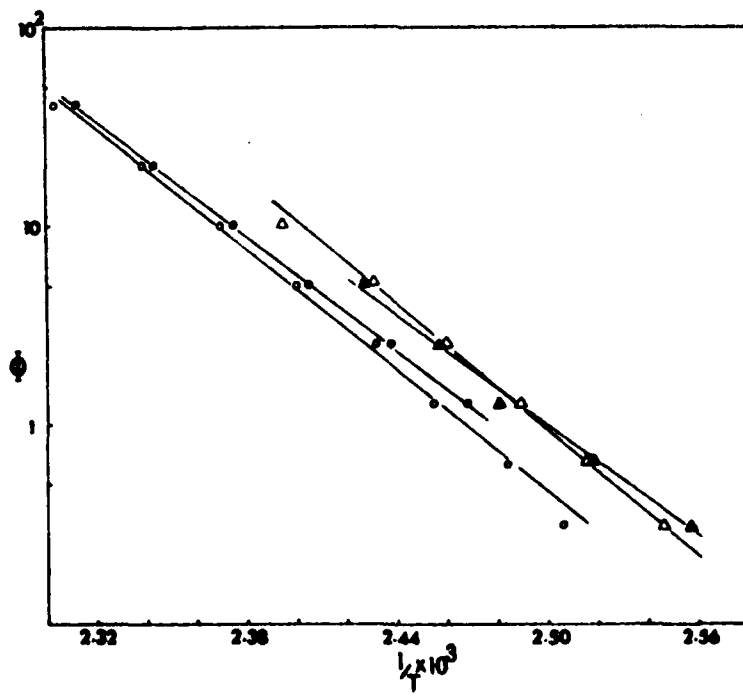
24

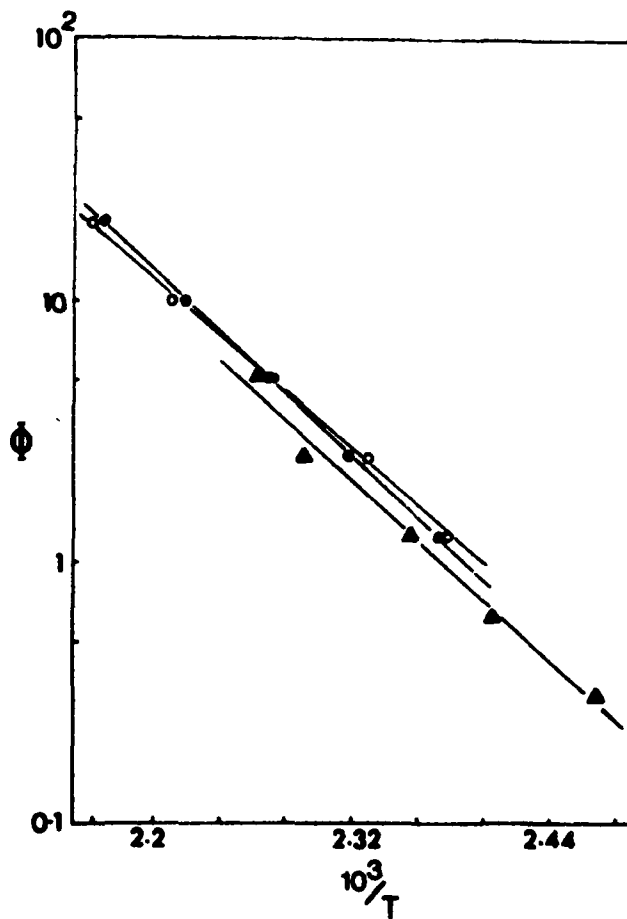


25

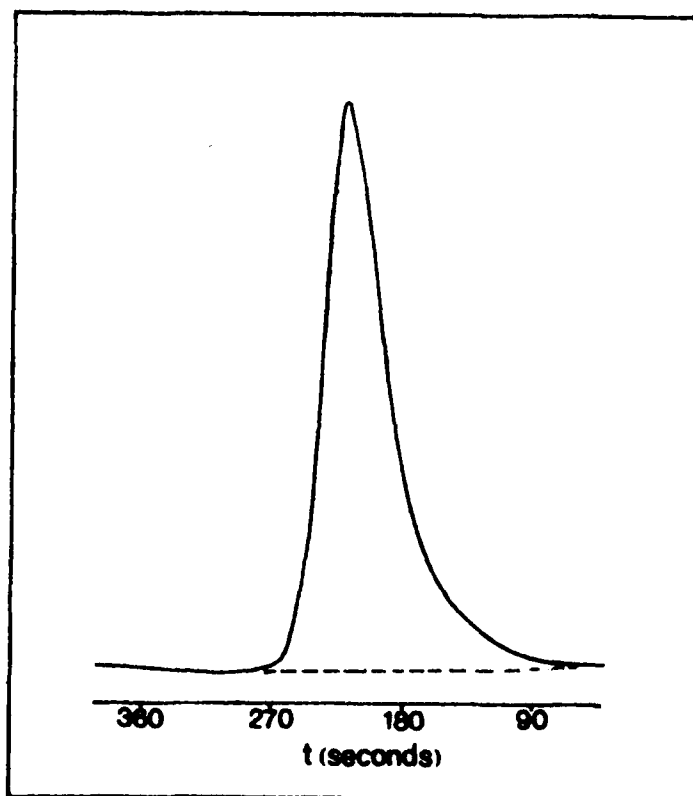


26

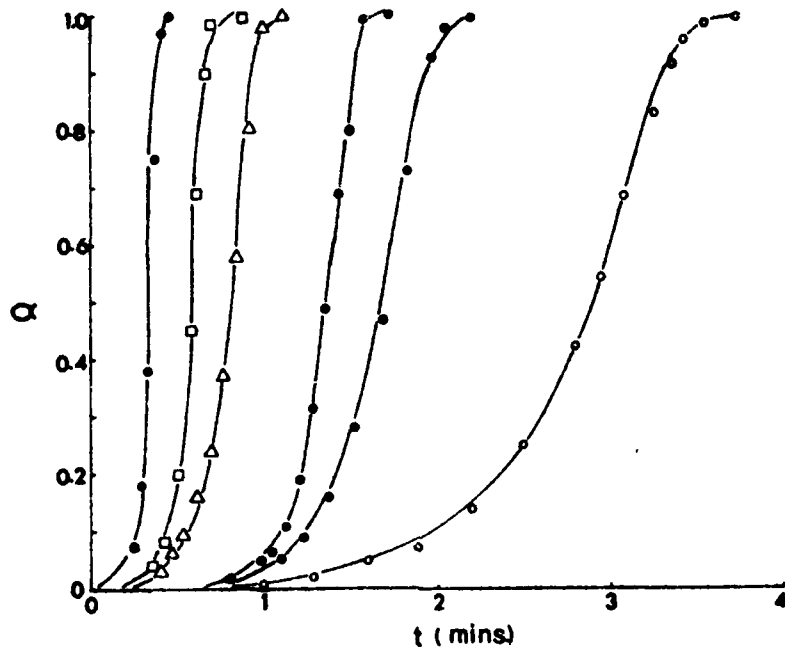




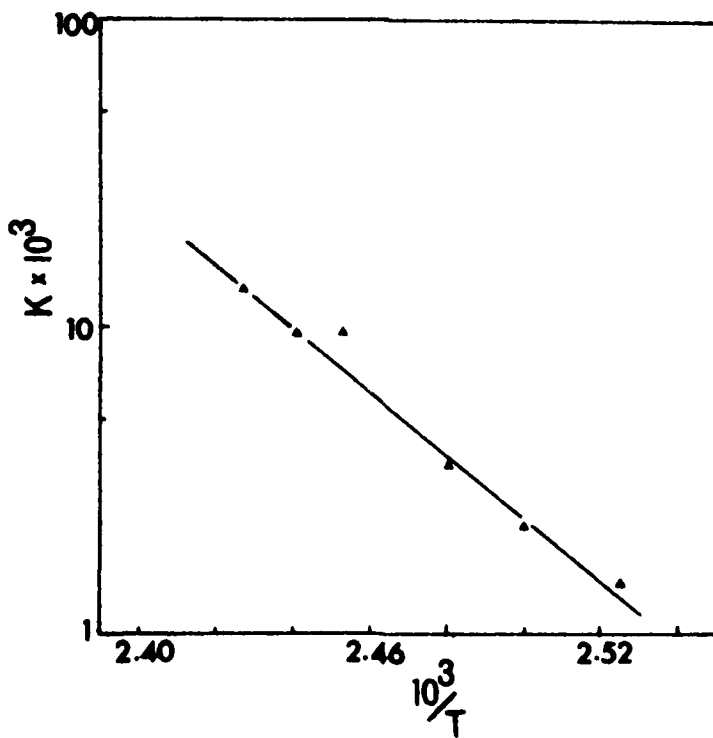
27



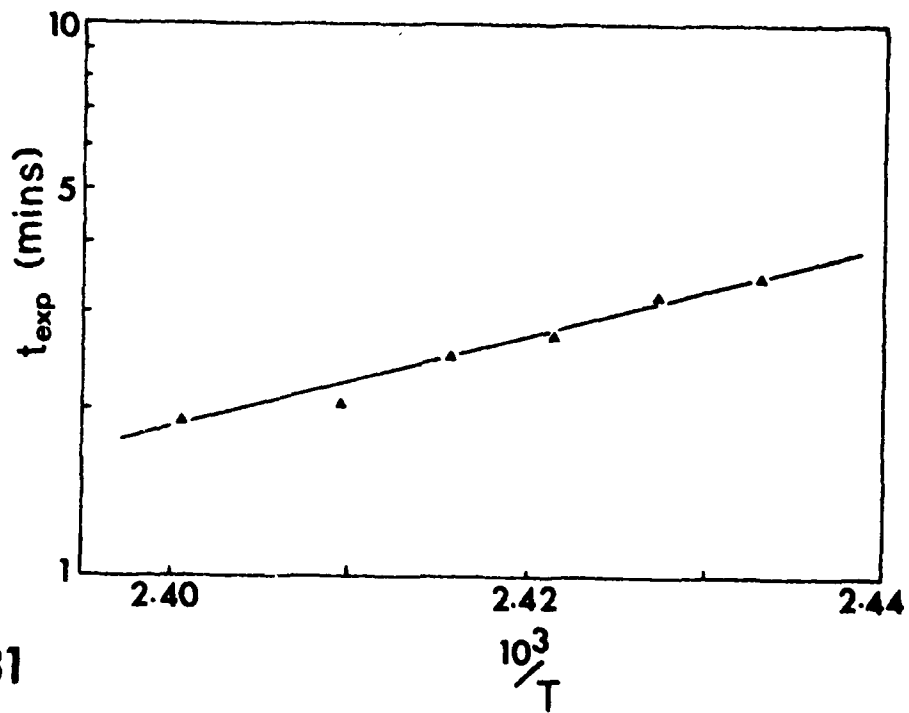
28



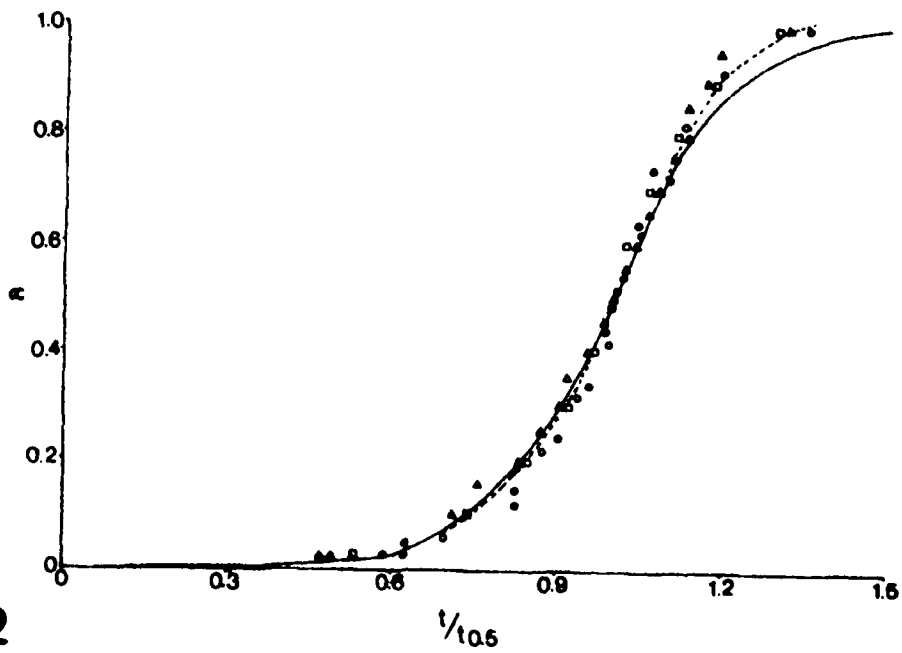
29



30



31



32